

## Interpretation of the Polarization of Venus

JAMES E. HANSEN

*Goddard Institute for Space Studies, New York, N. Y. 10025*

J. W. HOVENIER

*Dept. of Physics and Astronomy, Free University, Amsterdam, Netherlands*

(Manuscript received 20 November 1973, in revised form 15 January 1974)

### ABSTRACT

The linear polarization of sunlight reflected by Venus is analyzed by comparing observations with extensive multiple scattering computations. The analysis establishes that Venus is veiled by a cloud or haze layer of spherical particles. The refractive index of the particles is  $1.44 \pm 0.015$  at  $\lambda = 0.55 \mu\text{m}$  with a normal dispersion, the refractive index decreasing from  $1.46 \pm 0.015$  at  $\lambda = 0.365 \mu\text{m}$  to  $1.43 \pm 0.015$  at  $\lambda = 0.99 \mu\text{m}$ . The cloud particles have a narrow size distribution with a mean radius of  $\sim 1 \mu\text{m}$ ; specifically, the effective radius of the size distribution is  $1.05 \pm 0.10 \mu\text{m}$  and the effective variance is  $0.07 \pm 0.02$ . The particles exist at a high level in the atmosphere, with the optical thickness unity occurring where the pressure is about 50 mb.

The particle properties deduced from the polarization eliminate all but one of the cloud compositions which have been proposed for Venus. A concentrated solution of sulfuric acid ( $\text{H}_2\text{SO}_4\text{-H}_2\text{O}$ ) provides good agreement with the polarization data.

### 1. Introduction

Venus is our nearest planetary neighbor, yet one of the most mysterious. To a large extent this is due to the veil of clouds surrounding the planet. These clouds not only mask Venus, but their own composition is unknown. Many possible compositions have been suggested in the literature, including water,  $\text{H}_2\text{O}$  ice, solid  $\text{CO}_2$ , carbon suboxide ( $\text{C}_3\text{O}_2$ ; Sinton, 1953; Kuiper, 1957; Harteck *et al.*, 1963), hydrated ferrous chloride ( $\text{FeCl}_2 \cdot 2\text{H}_2\text{O}$ ; Kuiper, 1969),  $\text{NaCl}$  (Hunten, 1968), formaldehyde ( $\text{CH}_2\text{O}$ ; Wildt, 1940), hydrocarbons (Velikovsky, 1950; Hoyle, 1955; Kaplan, 1963), hydrocarbon-amide polymers (Robbins, 1964), polywater (Donahue, 1970), ammonium nitride ( $\text{NH}_4 \cdot \text{NO}_2$ ; Dauvillier, 1956), calcium and magnesium carbonates (Öpik, 1961),  $\text{NH}_4\text{Cl}$  (Lewis, 1968; Hunten and Goody, 1969), mercury and mercury compounds (Lewis, 1969; Rasool, 1970) and aqueous solutions of hydrochloric acid ( $\text{HCl} \cdot n\text{H}_2\text{O}$ ; Lewis, 1972; Hapke, 1972) and sulfuric acid ( $\text{H}_2\text{SO}_4 \cdot n\text{H}_2\text{O}$ ; Sill, 1972; Young and Young, 1973; Young, 1973). Although a large amount of theoretical and observational effort has been expended on this problem, no consensus on the cloud composition has evolved.

Our best means for investigating the clouds of Venus still is through measurements of reflected sunlight. The spectral reflectivity of Venus exhibits strong absorption features in the near-infrared ( $\lambda \approx 3 \mu\text{m}$ ) and in the ultraviolet ( $\lambda \lesssim 0.35 \mu\text{m}$ ) which a proposed cloud

material should be consistent with. However, these features have proved insufficient for either a specific identification of the cloud particles or eliminating most proposed compositions, in part because it is always possible to hypothesize a gaseous absorber, an admixture of another cloud material, or a lower cloud layer to provide the observed absorption. There have been concerted attempts to link several weaker features in the spectral reflectivity to specific cloud compositions, particularly  $\text{H}_2\text{O}$  ice (Sagan and Pollack, 1967) and  $\text{FeCl}_2 \cdot 2\text{H}_2\text{O}$  (Kuiper, 1969); however, the features which were associated with ice (other than the absorption at  $\lambda \approx 3 \mu\text{m}$ ) have also been credited to gaseous  $\text{CO}_2$  absorption (cf. Rea and O'Leary, 1968), and a number of the features associated with ferrous chloride are of doubtful reality (cf. Cruikshank and Thomson, 1971).

A different sort of evidence on the cloud composition is provided by the angular distribution of reflected light, both the distribution of brightness over the planetary disk and the disk-integrated brightness as a function of planetary phase angle. Arking and Potter (1968) analyzed such observations for Venus by comparing them with multiple scattering computations for spherical cloud particles. They found agreement with the observations for micron-sized or larger transparent spheres with a real refractive index  $1.33 \lesssim n_r \lesssim 1.7$  for visible wavelengths. This conclusion depends on the *assumption* that the particles are spherical, and further-

more the derived range for the refractive index includes practically all of the compositions which have been suggested for the Venus cloud particles.

Polarization observations are more sensitive to cloud particle characteristics than are brightness observations (cf. Hansen, 1971b) and thus the polarization offers a potentially powerful tool for investigating the nature of the Venus clouds. High quality polarization observations of Venus were obtained by Lyot (1929) for visual light and extended throughout the range  $0.35 \lesssim \lambda \lesssim 1 \mu\text{m}$  by Dollfus (1966) and Coffeen and Gehrels (1969). Semi-quantitative analyses of the polarization were made by Lyot (1929) on the basis of laboratory comparisons and by Coffeen (1968, 1969), Sobolev (1968) and Loskutov (1971) on the basis of single scattering computations for spheres. The most complete of these analyses is that of Coffeen, in which he found that the available observations were compatible with spheres of radius  $1.25 \pm 0.25 \mu\text{m}$  and refractive index  $1.43 \leq n_r \leq 1.55$ . Nonspherical particles were not excluded by the analysis of Coffeen and no attempt was made to investigate the influence of the particle size distribution on the conclusions.

The major task required in a quantitative analysis of the polarization is a proper accounting for multiple scattering. Horak (1950) made accurate multiple scattering computations for Rayleigh scattering, based on the theory of Chandrasekhar (1950), but he found that Rayleigh scattering did not resemble Lyot's polarization observations of Venus. Hansen and Hovenier (1971) made accurate computations with the doubling method (Hansen, 1971a; Hovenier, 1971) for scattering by cloud particles; their results demonstrated the large effect of multiple scattering on the polarization. Kattawar *et al.* (1971) made multiple scattering computations with the approximate Monte Carlo method for a spherical atmosphere and concluded that the cloud particles in the highest cloud layer on Venus have a refractive index  $1.45 \lesssim n_r \lesssim 1.60$ . Hansen and Arking (1971) made computations with the doubling method for comparison with observations of Lyot (1929) and Coffeen and Gehrels (1969) at three wavelengths; the results showed that the cloud particles on Venus are spherical with refractive index  $1.45 \pm 0.02$  and mean radius  $\sim 1 \mu\text{m}$  and that the cloud-top pressure level is  $\sim 50$  mb.

In this paper we report the results of a series of computations much more extensive than those of Hansen and Arking (1971). Many observations not included by Hansen and Arking (Kuiper, 1957; Marin, 1965; Dollfus, 1966; Dollfus and Coffeen, 1970; Forbes, 1971; Veverka, 1971) are incorporated in this study, and observations at all available wavelengths are analyzed. In addition, a detailed documentation of the method of analysis is included, and the refractive index dispersion derived from the polarimetric data is compared with dispersions of proposed cloud compositions.

## 2. Single scattering

Theoretical calculations for scattering by a planetary atmosphere are conveniently divided into two parts: single scattering by small volume elements in the atmosphere with optical thickness much less than unity and multiple scattering by the complete model atmosphere with any optical thickness. For comparison to disk-integrated observations, the multiple scattering computations must also be integrated over the visible part of the disk, as described in Section 3.

Exact solutions for single scattering are feasible for spheres and particles of a few other shapes (cf. van de Hulst, 1957; Kerker, 1969; Kratochvil, 1964; Coffeen and Hansen, 1973). For practical applications computations are almost always made using spherical particles, and it is essential to realize the limitations that this places on conclusions which may be obtained. However, in some applications the observations are sufficient to prove that the particles being examined are in fact spherical. This turns out to be the case for the Venus clouds.

The solution for scattering of a plane wave by an isotropic homogeneous sphere was obtained by Mie (1908). The results for a single sphere depend on  $n_c$  and  $x$ , where  $n_c = n_r - in_i$  is the complex refractive index of the sphere relative to the surrounding medium, with  $i = (-1)^{1/2}$ , and  $x = 2\pi r/\lambda$  is the size parameter, with  $r$  the particle radius and  $\lambda$  the wavelength of the incident radiation. The theory for single scattering is described in detail by van de Hulst (1957); here we give only information required in the application to follow.

The single scattering quantities required for the multiple scattering computations are the single scatterings albedo  $\bar{\omega}_0$  and the phase matrix  $\mathbf{P}(\alpha)$ , where  $\alpha$  is the scattering angle ( $\alpha = 0$  for light scattered exactly in the forward direction). In the clouds of Venus  $\bar{\omega}_0$  must be very close to unity in the optical window to yield the observed high spherical (Bond) albedo, and an approximate value for  $\bar{\omega}_0(\lambda)$  can be estimated from the requirement of matching the observed spherical albedo. Thus, the major requirement for interpreting the polarization of Venus is a thorough knowledge of the dependence of the phase matrix on the particle refractive index and size distribution.

The phase matrix for a single sphere at a particular wavelength may be described by four functions of the radius and scattering angle,  $M_1(r, \alpha)$ ,  $M_2(r, \alpha)$ ,  $S_{21}(r, \alpha)$  and  $D_{21}(r, \alpha)$ , where we employ the notation of van de Hulst (1957). In the case of a size distribution of particles which scatter independently, the corresponding functions are obtained by integrating over all particles in the size distribution, e.g.,

$$M_1(\alpha) = \int_{r_1}^{r_2} \dot{M}_1(r, \alpha) n(r) dr, \quad (1)$$

where  $n(r)dr$  is the number of particles per unit volume

with radius between  $r$  and  $r+dr$ , and  $r_1$  and  $r_2$  are the smallest and largest particles in the size distribution.

The normalized phase matrix for spheres, defined with respect to the Stokes parameters  $\{I, Q, U, V\}$ , has the form

$$\mathbf{P}(\alpha) = \begin{pmatrix} P^{11} & P^{21} & 0 & 0 \\ P^{21} & P^{22} & 0 & 0 \\ 0 & 0 & P^{33} & -P^{43} \\ 0 & 0 & P^{43} & P^{33} \end{pmatrix}, \quad (2)$$

where

$$\left. \begin{aligned} P^{11}(\alpha) &= c[M_2(\alpha) + M_1(\alpha)]/2 \\ P^{21}(\alpha) &= c[M_2(\alpha) - M_1(\alpha)]/2 \\ P^{33}(\alpha) &= cS_{21}(\alpha) \\ P^{43}(\alpha) &= cD_{21}(\alpha) \end{aligned} \right\}, \quad (3)$$

and  $c$  is a constant defined such that the phase function  $P^{11}(\alpha)$  is normalized as

$$\frac{1}{4\pi} \int_{4\pi} P^{11}(\alpha) d\omega = 1, \quad (4)$$

where  $d\omega$  is an element of solid angle.

The phase matrix  $\mathbf{P}(\alpha)$  may be computed from Mie theory for any refractive index, wavelength and size distribution of spheres. But in the case of remote measurements of scattered light, such as Earth-based observations of Venus, the size distribution of particles is unknown. Thus to "invert" such measurements and obtain cloud particle properties it is essential to make a systematic analysis of the effect of the size distribution on the scattered light, as we describe here.

It is common practice to describe a distribution function by its moments, or parameters simply related to the moments, e.g., the mean, the variance, the skewness, etc. To facilitate the inversion of radiation measurements these parameters should be chosen such that the number required to describe an arbitrary particle size distribution is as small as possible. Clearly the first parameter should be some measure of the mean particle size. The simple arithmetic mean is

$$\langle r \rangle = \frac{\int_{r_1}^{r_2} rn(r) dr}{\int_{r_1}^{r_2} n(r) dr} = \frac{1}{N} \int_{r_1}^{r_2} rn(r) dr, \quad (5)$$

where  $N$  is the total number of particles per unit volume. However, a sphere of size  $r \gtrsim \lambda$  scatters an amount of light approximately proportional to its area,  $\pi r^2$ , and for smaller particles the amount of scattered light is proportional to an even higher power of the particle radius, reaching  $r^6$  for Rayleigh scatterers.

Thus, as the first parameter describing the size distribution, we use the *effective radius*, defined as

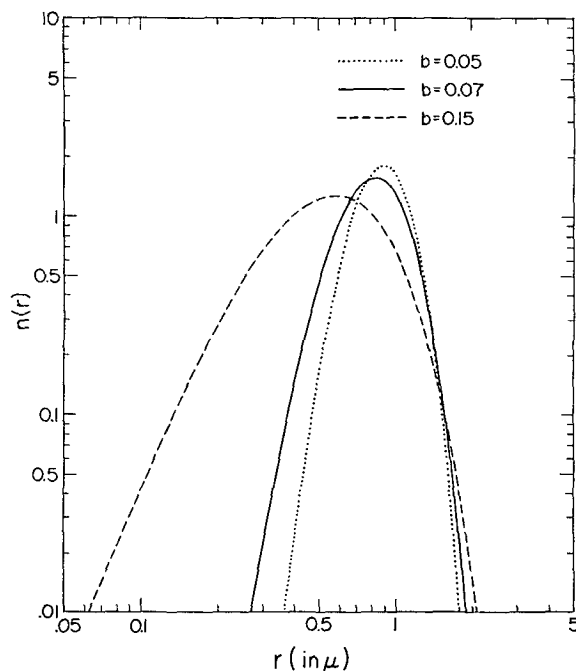


FIG. 1. Size distribution (8) for three values of  $b$ , where  $b$  is the effective variance. All three curves have  $a = 1.05 \mu\text{m}$ , where  $a$  is the effective radius. The mode radius, where  $n(r)$  is a maximum, is given by  $a(1-3b)$ . The distributions are normalized such that the integral over all sizes is unity.

$$r_{\text{eff}} = \frac{\int_{r_1}^{r_2} r\pi r^2 n(r) dr}{\int_{r_1}^{r_2} \pi r^2 n(r) dr}. \quad (6)$$

Similarly, as a measure of the width of the size distribution, we use the *effective variance*, defined as

$$v_{\text{eff}} = \frac{\int_{r_1}^{r_2} (r - r_{\text{eff}})^2 \pi r^2 n(r) dr}{r_{\text{eff}}^2 \int_{r_1}^{r_2} \pi r^2 n(r) dr}, \quad (7)$$

where  $r_{\text{eff}}^2$  in the denominator makes  $v_{\text{eff}}$  dimensionless.

This procedure can be continued to higher moments. However, for many purposes  $r_{\text{eff}}$  and  $v_{\text{eff}}$  are adequate for describing the size distribution. This has been demonstrated, for example, in computations by Hansen (1971b) for measured size distributions of terrestrial water clouds and for the analytic distribution

$$n(r) = \text{constant} \times r^{(1-3b)/b} e^{-r/ab} \quad (8)$$

with the same values of  $r_{\text{eff}}$  and  $v_{\text{eff}}$ . The close similarity of the results for the measured and analytic distributions shows that these two parameters define the major

characteristics in the intensity and polarization as a function of scattering angle.

In the computations for this paper we also use the distribution (8) because it has the simple property that

$$\left. \begin{aligned} a &= r_{\text{eff}} \\ b &= v_{\text{eff}} \end{aligned} \right\},$$

provided the integrations in (6) and (7) extend over all particles ( $r=0, \infty$ ). Distribution (8) is a form of the gamma distribution (cf. Kendall and Stuart, 1963); other variations have been extensively used for cloud particle size distributions, e.g., by Khrigian (1961) and Deirmendjian (1964). The constant in (8) is related to

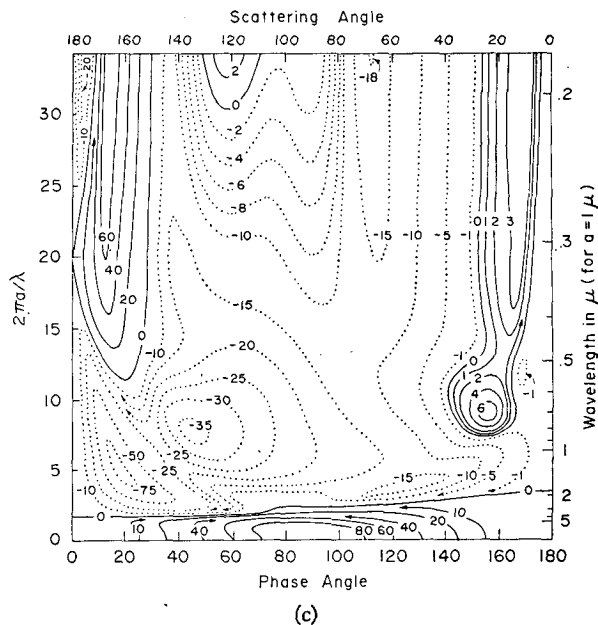
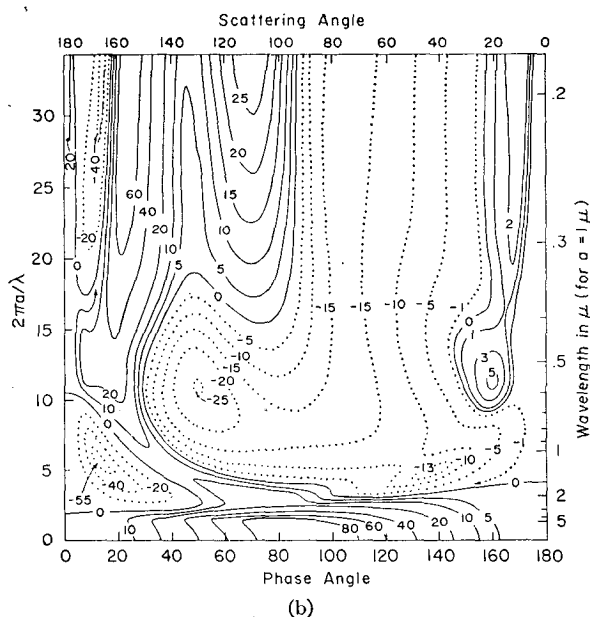
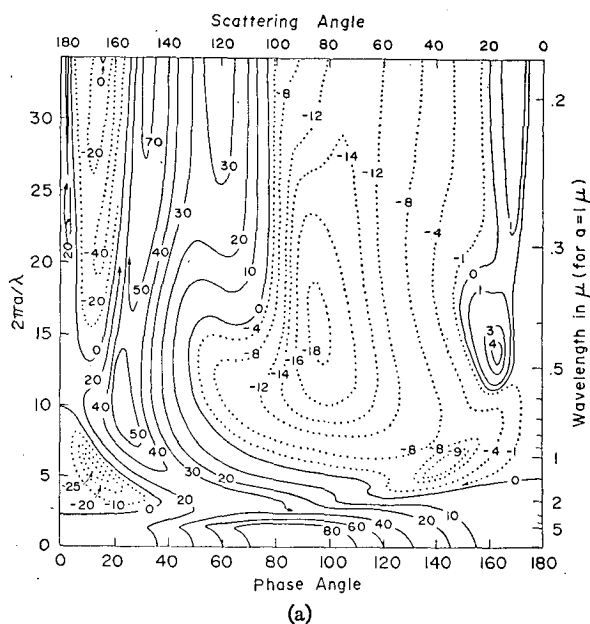


Fig. 2. Percent polarization,  $-100P^{21}/P^{11}$ , for single scattering of unpolarized incident light by a size distribution of spheres. Solid lines indicate positive polarization and dotted lines negative polarization. The three parts of the figure show results for three real refractive indices,  $n_r=1.33$ (a), 1.40(b) and 1.50(c). The size distribution is that given by (8) with  $b=0.05$  in all three cases. The wavelength scale applies for the choice  $a=1 \mu$ .

the total number density of particles per unit volume,  $N$ , by

$$\text{constant} = N(ab)^{(2b-1)/b} / \Gamma[(1-2b)/b], \quad (9)$$

where  $\Gamma$  is the gamma function.

Fig. 1 shows three examples of distribution (8). All three have  $a=1.05 \mu$ , but  $b=0.05, 0.07$  and  $0.15$ , respectively. The maximum of  $n(r)$  occurs at  $r_m = a(1-3b)$ . The standard deviation for the distribution (8) is  $\sigma = a[b(1-2b)]^{1/2}$ . For  $a=1.05 \mu$  and  $b=0.07$ , for example, we find  $r_m=0.83 \mu$  and  $\sigma=0.26 \mu$ .

The contour diagrams in Figs. 2 and 3 demonstrate the dependence of the single scattering polarization on the refractive index and size distribution. These diagrams show the percent polarization for single scattering of incident unpolarized light,  $-100P^{21}/P^{11}$ , as a function of phase angle (the supplement of the scattering angle) on the horizontal axis and as a function of the effective size parameter  $2\pi a/\lambda$  on the vertical axis. By choosing any fixed value for  $a$  the vertical scale can be converted to a scale for  $\lambda$ . This is done on the right side of each figure for the choice  $a=1 \mu$ ; the wavelength scale for a different choice of  $a$  can be obtained by multiplying the given scale by  $a$  (in  $\mu$ ). For any fixed wavelength  $\lambda$  the effective size parameter scale on the left can be converted to a scale for  $a$  by means of the multiplication factor  $\lambda/(2\pi)$ .

Fig. 2 illustrates the dependence of the polarization on the refractive index for three refractive indices in the

range previous studies have shown to be relevant to the clouds of Venus. Each of the three parts in Fig. 2 is for size distribution (8) with  $b=0.05$ . This distribution is broad enough to smooth out most of the interference maxima and minima which occur for a single particle, but not broader than naturally occurring distributions.<sup>1</sup>

The integration over size parameters extends from  $x_1=0$  to  $x_2=45.7$ . For the top part of Fig. 2 this is not equivalent to the range  $(0, \infty)$  which is required to make exactly  $r_{\text{eff}}=a$  and  $v_{\text{eff}}=b$ . For example, at  $2\pi a/\lambda=30$ ,  $2\pi r_{\text{eff}}/\lambda$  is  $\sim 29.3$  and  $v_{\text{eff}}$  is  $\sim 0.044$ ; however, the deviations of  $r_{\text{eff}}$  from  $a$  and  $v_{\text{eff}}$  from  $b$  are not sufficient to alter the conclusions we draw from the figure. The computations were made for 130 phase angles, 0.5(1)39.5(2)139.5(1)179.5, and 61 equally spaced effective size parameters in the interval  $(0, 34.3)$ . In the proximity of isolated maxima and minima of the polarization some additional computations were made. The accuracy with which the contours could be drawn is estimated to be close to the width of the lines in the figures.

For the smallest size parameters there is the strong positive polarization of Rayleigh scattering, with the maximum polarization at phase angle  $90^\circ$ . The Rayleigh scattering region is similar for the different refractive indices, but it is more compressed for the larger values of  $n_r$ ; this is understandable since the conditions for Rayleigh scattering are  $x \ll 1$  and  $|n_c x| \ll 1$ .

For the largest size parameters in Fig. 2 the polarization approaches that for geometrical optics (cf. van de Hulst, 1957; Liou and Hansen, 1971). At small scattering angles the polarization is small because of the predominance of unpolarized diffracted light. Other than diffraction, most of the light scattered in the forward hemisphere is due to rays passing through the particle with two refractions. This light is negatively polarized, as follows from Fresnel's equations. Reflection from the outside of the particles contributes a positive polarization at all phase angles; although the intensity of these rays is small, it is sufficient to cause the long peninsula of positive polarization at scattering angles  $\alpha \approx 15^\circ$ . This feature becomes stronger as  $n_r$  increases, because the Fresnel reflection coefficients increase with  $n_r$ .

The steep ridge and positive polarization maximum at scattering angles  $\sim 150^\circ$  (for  $n_r=1.33$ ) is the primary rainbow. This arises from rays internally reflected one time in spheres. These rays tend to be concentrated at a given scattering angle, as can be shown from Snell's law and the Fresnel reflection coefficients. Similarly, the weaker feature at  $\alpha \approx 120^\circ$  (for  $n_r=1.33$ ) is the second rainbow, due to rays undergoing two internal reflections. Still higher rainbows contain a negligible fraction of the scattered light, and they do not contribute any noticeable feature in Fig. 2. The location of the rain-

bows in scattering angle varies with  $n_r$  in accordance with Snell's law.

The sharp maximum in the polarization in the back-scattering direction ( $\alpha \approx 180^\circ$ ) is the so-called glory. This is due in large part to incident edge rays (i.e., grazing rays) which set up surface waves on the scattering particle (van de Hulst, 1957; Bryant and Cox, 1966; Fahlen and Bryant, 1968). These surface waves spew electromagnetic energy in all directions, but it is focused in the forward direction, where it is lost in the stronger diffracted light, and in the backward direction, where it gives rise to the glory. For refractive indices in the range  $2^{1/2} \lesssim n_r \lesssim 2$  there is also a large contribution to the glory from rays internally reflected one time.

For scattering angles  $\sim 20^\circ$  and size parameters  $\sim 15$  (for  $n_r=1.33$ ) there is a hill of positive polarization, which nearly forms an island but is connected to the peninsula of positive polarization for larger particles. This feature is a manifestation of what van de Hulst (1957) calls "anomalous diffraction." It is due to optical interference between diffracted light and light reflected and transmitted by the particle in the near-forward direction. The phase shift of a ray traveling through the center of the sphere is  $\rho = 2x(n_r - 1)$ , which accounts for the location of this feature in size parameter varying approximately as  $1/(n_r - 1)$ .

In the transition region between large-particle scattering and Rayleigh scattering the polarization is a complicated function of size parameter. As the size parameter decreases the degree to which the paths of separate light rays can be localized decreases. Thus the second rainbow, with a more detailed ray path, is lost from the polarization before the primary rainbow is. With decreasing size parameter the primary rainbow becomes blurred and its peak first moves toward larger scattering angles due to the asymmetric shape of the rainbow. For  $n_r=1.33$  the peak of the primary rainbow shifts to smaller scattering angles for size parameters  $\lesssim 10$  and merges with Rayleigh scattering. This effect is less pronounced for the larger values of  $n_r$  because the Rayleigh region is more depressed and the rainbow is at a scattering angle further from the Rayleigh maximum. The negative polarization features for size parameters  $\sim 5$  are due to edge rays and resulting surface waves, i.e., they are "glory" phenomena. The angular size of the region into which the glory is focused increases inversely with the size parameter.

Fig. 3 shows the polarization for  $n_c=n_r=1.44$  and the size distribution (8) with  $b=0.05$ , 0.07 and 0.15. The integration limits on  $x$  for these three cases were  $(0, 34.3)$ ,  $(0, 34.3)$  and  $(0, 68.6)$ , respectively. For the top part of the figure these integration limits are not equivalent to  $(0, \infty)$ . Nevertheless, the differences which would exist in the polarization if we used the limits  $(0, \infty)$  are small enough that none of our conclusions are affected by the finite integration limits. The calculations were for the same phase angles and size parameters as for Fig. 2.

<sup>1</sup> Typical values of  $v_{\text{eff}}$  for terrestrial atmospheric particles are (Hansen and Travis, 1974): 0.05–0.4 for water clouds, 0.5–20. for tropospheric hazes, and 0.05–0.1 for the particles in the aerosol layer near 20 km (Junge layer).

Fig. 3 thus illustrates the effect of the width of the size distribution on the polarization. The qualitative effect of broadening the distribution is easy to understand: it roughly corresponds to taking averages along vertical lines. Thus, with increasing  $b$  hills tend to be smoothed out, holes are filled in, and corners are rounded off; straight vertical lines, however, remain essentially unchanged.

The feature of anomalous diffraction (at  $2\pi a/\lambda \approx 10$ ,  $\alpha \approx 20^\circ$ ) is one of the most sensitive to the particle size distribution. Its maximum polarization is almost cut in half as  $b$  increases from 0.05 to 0.07, and the feature is washed away for  $b=0.15$ . This is understandable since only a narrow distribution of sizes has the phase shift required for the interference feature.

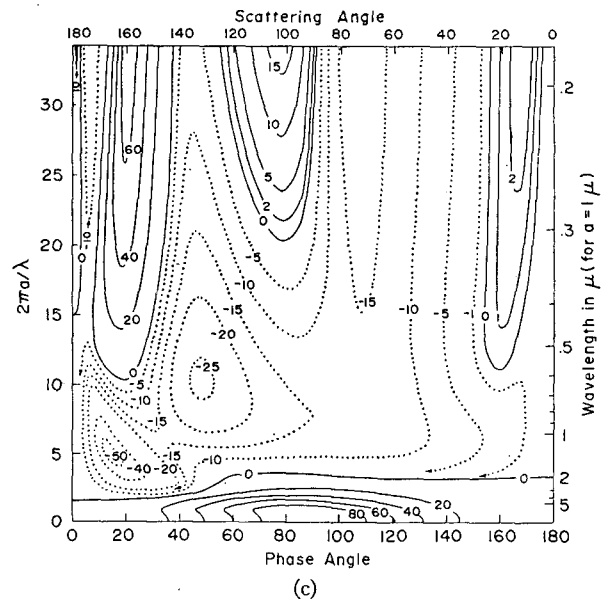
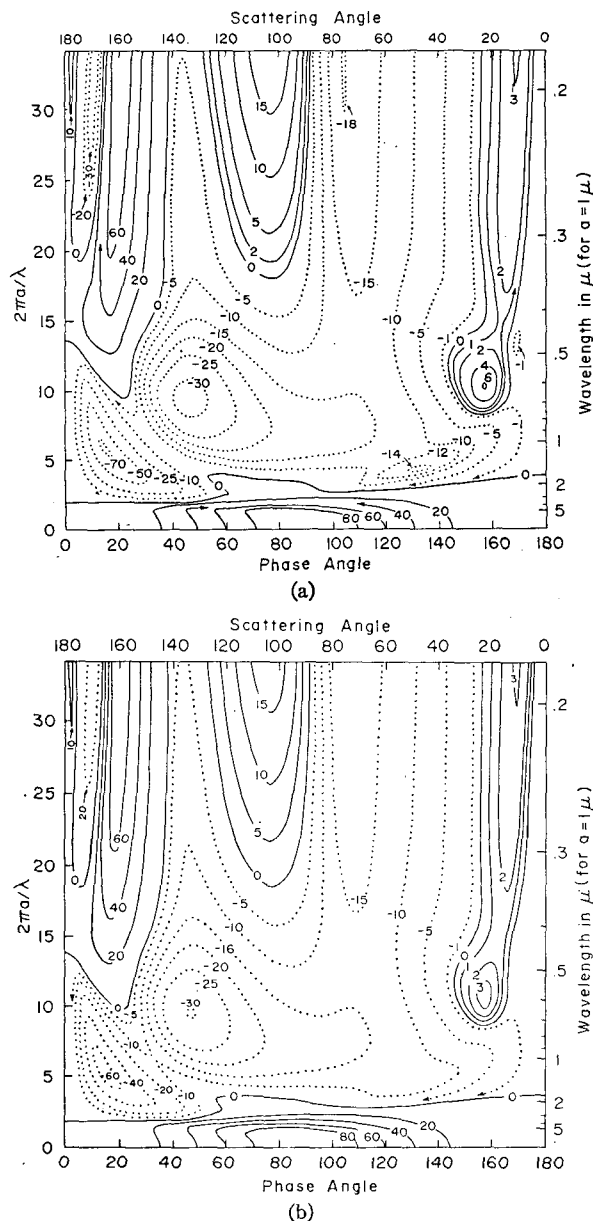


FIG. 3. Percent polarization for single scattering of unpolarized incident light by a size distribution of spheres,  $-100P^{21}/P^{11}$ . As in Fig. 2 except that the three parts of the figure show results for three effective variances,  $b=0.05$  (a),  $0.07$  (b) and  $0.15$  (c) with  $n_r=1.44$  in all three cases.

The bridge of positive polarization formed by the merging of the primary rainbow and Rayleigh scattering (e.g., for  $n_r=1.33$  and  $1.40$  in Fig. 2) is also strongly affected by the width of the size distribution. For  $n_r=1.33$  and  $b=0.05$  the polarization is positive for all size parameters at scattering angles  $\sim 140^\circ$ ; thus, for any broader size distribution the polarization for single scattering must be positive at  $\alpha \approx 140^\circ$ . On the other hand, it is apparent that for  $n_r=1.40$  the bridge will be eroded away for a broad distribution. We have verified this with computations for  $b=0.16$  which show a breach of negative polarization with a vertical extent of  $\sim 1.3$  in size parameter. The extent of this breach increases for larger  $b$ .

The existence or non-existence of the bridge of positive polarization is important for the application to Venus. Coffeen (1969) has noted that at  $\lambda=1 \mu$  the polarization of Venus is negative for all phase angles. By making the assumption that multiple scattering does not change the sign of the polarization from that which exists for single scattering, Coffeen concluded that for the Venus cloud particles  $n_r \geq 1.43$ , since his computations showed the existence of the bridge for smaller  $n_r$ . However, his computations were all for a very narrow size distribution, with  $v_{\text{eff}}=1/48 \approx 0.02$ . If  $v_{\text{eff}}$  is permitted to be as large as for terrestrial clouds and the other assumptions of Coffeen are kept, it can only be concluded that the lower limit on the refractive index is  $n_r \gtrsim 1.37$ .

Lyot (1929) and Coffeen (1969) noted that the qualitative effect of multiple scattering on the polariza-

tion is to reduce the degree of polarization without changing its sign. Thus, the features in the single scattering described above are useful for interpreting the polarization of scattered light, even for a thick atmosphere. Hansen and Hovenier (1971), however, found from accurate computations that the polarization of multiple-scattered photons is not negligible, particularly for photons which are scattered only two or three times. In the case of cloud particles which are comparable to or larger than the wavelength, the polarization of photons emerging from the atmosphere after just a few scatterings is qualitatively similar to the polarization for single scattering. This is a result of the fact that many photons are scattered in the forward direction on the first one or two scatterings at which time they are still nearly unpolarized, and then they are scattered out of the atmosphere on their next scattering. Such photons have a polarization similar to that for single scattering, but with the features somewhat smeared out as a function of phase angle [cf. Figs. 24 and 25 of Hansen (1971b) and the accompanying explanation]. Thus, multiple scattering, in addition to reducing the degree of polarization, causes a smoothing of the polarization along horizontal lines in Figs. 2 and 3. This smoothing is less pronounced than that along vertical lines due to the distribution of particle sizes; furthermore, it is fully accounted for by an exact multiple scattering theory.

All the computations we have illustrated pertain to spheres. For small nonspherical particles there would also be a region of Rayleigh scattering. For large size parameters the same division of rays into diffracted, reflected and refracted components can be made as in the case of spheres. However, the polarization for most of these components will, in general, be quite different than for spheres. Rainbows, for example, depend on the particle having a circular cross section; thus, long circular cylinders cause a rainbow, and for such cylinders oriented perpendicular to the incident light the polarization of the rainbow is very similar to that for spheres (cf. Liou, 1972). The glory requires a spherical particle shape; this is clear from the physical origin of the glory and it is illustrated, for example, by computations for circular cylinders (Liou, 1972) and by the absence of a glory for terrestrial ice clouds. The feature of anomalous diffraction would be smoothed away by an irregular particle shape or by a random orientation of any nonspherical particles in the same way that it is smoothed away by a broad size distribution; this is because the path length through the particle must have a fixed relation to the path length outside the particle.

Nonspherical particles with a regular shape may give rise to specific polarization features of their own. For example, large hexagonal ice crystals ( $n_r=1.31$ ) yield a concentration of negatively polarized light at  $\alpha \approx 22^\circ$ , the so-called  $22^\circ$  halo (cf. Minnaert, 1954; O'Leary, 1966). Similarly a  $90^\circ$  crystal interface causes a  $46^\circ$  halo for ice crystals. Usually, however, there is a distribution

of particle orientations and particle shapes; this tends to average out sharp angular features in the polarization. Laboratory observations (e.g., Lyot, 1929; Huffman, 1970) and airborne observations of ice clouds (Coffeen and Hansen, 1973; Coffeen *et al.*, 1974) tend to verify that the polarization for nonspherical particles is a smoother function of scattering angle than it is for spheres.

The computations we have illustrated are for a real refractive index, i.e., for  $n_i=0$ . This is sufficient for application to the visible clouds of Venus, as is shown in the next section.

### 3. Multiple scattering

The computations which we present in this paper are for the simplest possible relevant model: a homogeneous locally-plane-parallel atmosphere. It is preferable to fully investigate this model before adding complications such as vertical and horizontal inhomogeneities. Indeed, with a thorough understanding of this model in hand the general effects of such complications can be anticipated, as is discussed below and in Section 5.

Our multiple scattering computations were made with the doubling method. van de Hulst (1963) developed this method in essentially the form which we use, but without polarization; it was extended to include polarization by Hansen (1971a) and Hovenier (1971). The method provides a prescription for obtaining the reflection and transmission matrices for an atmosphere composed of two layers from the reflection and transmission matrices for each of the component layers. Thus, by choosing the two layers to be identical a thick atmosphere can be built up geometrically. The dependence on azimuth was handled by means of Fourier series expansions. Complete formulas are given in the above references.

In most of our computations we began the doubling at an optical thickness  $\tau_0=2^{-15}$ , with the reflection and transmission matrices for the layer of this thickness obtained from equations for first-order and second-order scattering (Hovenier, 1971). In some computations  $\tau_0$  was chosen as  $2^{-20}$  which is sufficiently small for only single scattering to be employed for this layer. These initial optical thicknesses and the number of Gauss points used in the integrations over angle were adequate to allow a final accuracy comparable to the thickness of the curves in the figures for polarization versus phase angle. Some of the checks which we have made on the accuracy are listed by Hansen and Hovenier (1971).

In principle, the computations should employ phase matrices of four rows and four columns [cf. (2)]. However, for the case of spherical particles and incident unpolarized light, Hansen (1971b) has shown that the error in the degree of polarization for multiple scattered light is  $\lesssim 0.00002$  for the approximation obtained by setting  $P^{43}=0=P^{34}$ . This error, of course, is negligible for our purposes, and thus in our computations we

included only the first three rows and columns in the phase matrices and reflection and transmission matrices.

Most of the polarization observations of Venus refer to the total light from the visible part of the planetary disk. Thus, we integrated the results of our multiple scattering computations over the planetary disk, assuming a spherical but locally-plane-parallel atmosphere. Only at large phase angles is the neglect of atmospheric curvature of possible significance, and computations with the Monte Carlo method (Kattawar and Adams, 1971; Collins *et al.*, 1972) indicate that even at these phase angles the difference in polarization is small between the locally-plane-parallel model and the model accounting for curvature. Cloud bumpiness or waviness may have an effect at large phase angles at least comparable to that of atmospheric curvature (cf. Öpik, 1962; van Blerkom, 1971); if such effects exist it is not clear whether a model accounting for curvature or a locally-plane-parallel model is more accurate. However, single scattering strongly dominates in the polarization for large phase angles and thus the choice of model is probably not very important. The disk integration was performed at about 50 phase angles in the range 0–180°, the exact values of the phase angles being more concentrated near sharp features in the polarization.

We basically followed the disk-integration method of Horak (1950), which involves a double-quadrature, or “cubature,” over the visible disk. The Stokes parameters of the reflected radiation were evaluated at each of the cubature points by linear interpolation from the Stokes parameters computed at the Gauss divisions with the doubling method. At small phase angles ( $\alpha \lesssim 20^\circ$ ) the interpolation did not yield sufficiently accurate results at the cubature points; this difficulty was overcome by employing certain integral equations satisfied by the reflection matrix [cf. Chandrasekhar (1950, p. 169) and correction indicated by Hovenier (1969, p. 493)] to improve the accuracy of the Stokes parameters at the cubature points. The procedure is similar to that described by Horak and Little (1965) for unpolarized light. The accuracy of the disk integration was tested by comparison with Horak’s results, by comparison with the analytic solution for a Lambert surface, by computations for cases involving only single scattering, and by varying the number of cubature and Gauss points. Most of the final computations were made with 50-point cubature over half of the visible disk. In the figures which we present, the accuracy should be comparable to the thickness of the lines.

In most of our computations we took the optical thickness of the atmosphere to be  $\tau = \infty$  and chose the single scattering albedo  $\tilde{\omega}_0$  to yield the observed spherical albedo of Venus.<sup>2</sup> The value of  $\tilde{\omega}_0$  required to

<sup>2</sup> Computations with the doubling method were actually stopped at  $\tau = 256$ , which for all practical purposes was equivalent to  $\tau = \infty$ .

yield the spherical albedo  $A$  can be found for any phase matrix without iteration as follows. Table A1 of Chamberlain and Smith (1970) gives the value  $\tilde{\omega}_0^{\text{iso}}$  which will yield the spherical albedo  $A$  for isotropic scattering with  $\tau = \infty$ . The similarity relation (Hansen, 1969; van de Hulst and Grossman, 1968)

$$\tilde{\omega}_0 = 1 - (1 - \tilde{\omega}_0^{\text{iso}})(1 - \langle \cos \alpha \rangle) \quad (10)$$

then yields the required single scattering albedo;  $\langle \cos \alpha \rangle$  is the asymmetry parameter of the phase matrix for which  $\tilde{\omega}_0$  is required. The simple form of the similarity relation (10) is sufficient if  $(1 - \tilde{\omega}_0) \ll 1$  as is the case for Venus.

We numerically verified that the polarization in the above case is practically indistinguishable from the case  $\tilde{\omega}_0 = 1$  with the ground albedo zero and  $\tau$  chosen to yield the observed spherical albedo. With a homogeneous atmosphere, and the phase matrix and spherical albedo of the planet fixed, the only way a significantly different polarization could be obtained is with a thin atmosphere (and a high ground albedo). But  $\tau$  must be large for the Venus atmosphere; measurements by the Soviet spacecraft Venera 8 of sunlight transmitted by the atmosphere of Venus (Avduevsky *et al.*, 1973) indicate that the cloud optical thickness is  $\tau_c \gtrsim 10$  (Lacis and Hansen, 1974). The model-insensitivity of the polarization for a fixed phase matrix and planetary albedo is easy to understand. The degree of polarization is the ratio of the intensity of polarized light to the total intensity,  $I_{\text{pol}}/I$ . The total intensity  $I$  is essentially determined by the spherical albedo and the phase function in the upper part of the atmosphere;  $I_{\text{pol}}$  is determined by photons scattered not more than a few times, i.e., by the phase matrix in the upper part of the atmosphere.

Most of the phase matrices we employed were computed for real refractive indices, i.e., for  $n_i = 0$ . This special case is sufficient for the following reasons. The high albedo of Venus throughout the region  $0.4 \lesssim \lambda \lesssim 2.5 \mu\text{m}$  requires that the cloud particles have either a very small value of  $n_i$  or such a large refractive index that they are essentially “metallic.” In the latter case, however, the polarization would be entirely different from that which is observed for Venus, as has been noted by Coffeen (1969). To test the possible effect of small values of  $n_i$  on the polarization we found by iterative calculations the value of  $n_i$  required to yield the  $\tilde{\omega}_0$  corresponding to the assumed spherical albedo of Venus. This exercise was performed once for  $\lambda = 0.55 \mu\text{m}$  and once for  $\lambda = 0.365 \mu\text{m}$ . At all phase angles the polarization, graphed as in Figs. 4–12, was indistinguishable from the case in which the phase matrix was computed for  $n_i = 0$ .

Thus, the phase matrix for the cloud particles on Venus depends on the real refractive index  $n_r$  and the particle size distribution, as discussed in Section 2. For the size distribution (8), which is sufficient to represent the major characteristics of most naturally occurring

distributions, the two parameters are the effective radius  $a$  and the effective variance  $b$ . In addition, the phase matrix for a unit volume of the atmosphere depends on the ratio of the Rayleigh scattering coefficient (per unit length) to the cloud particle scattering coefficient, i.e.,

$$f = \frac{k_{sca,R}}{k_{sca,c}}, \quad (11)$$

and the complete phase matrix is

$$\mathbf{P} = \frac{1}{1+f} \mathbf{P}_c + \frac{f}{1+f} \mathbf{P}_R, \quad (12)$$

where  $\mathbf{P}_c$  and  $\mathbf{P}_R$  are the phase matrices for the cloud particles and for isotropic Rayleigh scattering.<sup>3</sup> In order to represent the Rayleigh contribution to the phase matrix in terms of a single wavelength-independent parameter we let  $f_R \equiv f(\lambda = 0.365 \mu\text{m})$ . At wavelengths other than  $0.365 \mu\text{m}$  we use<sup>4</sup>

$$f = \left[ \frac{0.365}{\lambda(\text{in } \mu\text{m})} \right]^4 f_R. \quad (13)$$

Thus, for our homogeneous model atmosphere the polarization at a particular wavelength is a function of  $n_r$ ,  $a$ ,  $b$  and  $f_R$ . Although the assumption of a homogeneous mixture of cloud particles and Rayleigh scatterers may be very inaccurate, this significantly affects the polarization only in the ultraviolet. The values derived for  $n_r$ ,  $a$  and  $b$  are independent of this assumption; only the number density of particles is uncertain.

We have made several hundred separate multiple scattering computations for comparison to available observations of Venus. In obtaining  $\bar{\omega}_0$  from (10) the assumed spherical albedo of Venus was based mainly on the intermediate-bandwidth photometric observations reported by Irvine (1968), and for  $\lambda = 0.55 \mu\text{m}$  also on the observations of Knuckles *et al.* (1961). The uncertainty in the spherical albedo is  $\sim 10\%$ . This translates into a comparable uncertainty in the degree of polarization,  $I_{pol}/I$ , since its only significant effect is on  $I$ . Thus, in most cases the variability in the theoretical polarization (for given  $n_r$ ,  $a$ ,  $b$ ,  $f_R$ ) due to the uncertainty in the spherical albedo is not more than

<sup>3</sup> With this phase matrix we are still able to account for the effects of anisotropic Rayleigh scattering, as discussed below and in Appendix A.

<sup>4</sup> Eq. (13) follows from the assumption that  $\sigma_R$  is proportional to  $\lambda^{-4}$  and  $\sigma_c$  is independent of wavelength for the region in which polarization observations are available and  $f$  is significant ( $0.34 \leq \lambda \leq 0.6 \mu\text{m}$ ). The first assumption is sufficiently accurate for most gases including  $\text{CO}_2$ . The accuracy of the second assumption depends on the particle size distribution; however, we made several computations in which the variation of  $\sigma_c$  with  $\lambda$  was accounted for (using the Mie theory) and we found that this affected the final polarization by at most a few tenths percent polarization.

TABLE 1. Examples of the single scattering albedo which approximately yield a given spherical albedo for the case  $a = 1.05 \mu\text{m}$ ,  $b = 0.07$ ,  $f_R = 0$ .  $\langle \cos \alpha \rangle$  was computed from Mie theory and  $\bar{\omega}_0$  from (10).

$\lambda$ ( $\mu\text{m}$ )	$n_r$	$\langle \cos \alpha \rangle$	$A$	$\bar{\omega}_0$
0.99	1.43	0.715	0.90	0.99941
0.55	1.44	0.718	0.87	0.99897
0.365	1.46	0.761	0.55	0.98427

a few tenths percent polarization. Table 1 shows the values of  $\bar{\omega}_0$  employed at three wavelengths for the case  $a = 1.05 \mu\text{m}$ ,  $b = 0.07$  along with the computed spherical albedos for the case  $f_R = 0$ . Since  $\bar{\omega}_0$  was not changed for other values of  $f_R$ , the computed spherical albedo in the ultraviolet increased slightly with increasing  $f_R$ ; for example, for  $f_R = 0.045$  the computed spherical albedo at  $\lambda = 0.365 \mu\text{m}$  is  $\sim 58\%$ . The wavelengths in Table 1 are those employed in most of the graphs we present and they span the region containing most of the polarization observations. In the remainder of this section we present a number of the results selected to illustrate the dependence of the polarization on wavelength and on the parameters  $n_r$ ,  $a$ ,  $b$  and  $f_R$ .

#### a. Wavelength $\lambda = 0.55 \mu\text{m}$

We first present results for  $\lambda = 0.55 \mu\text{m}$  because this wavelength region is the most sensitive to the particle size and it is also sensitive to the refractive index. In Figs. 4–6 we include a Rayleigh contribution  $f_R = 0.045$  as derived from the ultraviolet observations. We have not varied  $f_R$  in these figures because the effect of Rayleigh scattering is sufficiently small at  $\lambda = 0.55 \mu\text{m}$  (it increases the polarization by  $\sim 1\%$  at phase angle  $90^\circ$ , compared with  $f_R = 0$ ) that variations due to the uncertainty in  $f_R$  ( $\sim 0.01$ ) are negligible.

The observations in Figs. 4–6 include those made by Lyot (1929) with a visual polarimeter in the 1920's; these have been reproduced in many publications during the last 50 years. Although they refer to a rather broad wavelength region ( $\sim 800 \text{ \AA}$  full-width at half-maximum for a completely dark-adapted eye), they are in good agreement with the other observations which were made with intermediate-bandwidth filters [ $\sim 600 \text{ \AA}$  at  $\lambda = 0.55 \mu\text{m}$  (cf. Coffeen and Gehrels, 1969)]. All of the calculations are for a single wavelength. The finite bandwidth of the filters is essentially equivalent to an integration over size parameter, but the width of the intermediate bandwidth filter is sufficiently small that it should not have a major impact on the interpretations. Furthermore, a quantitative analysis shows that accounting for the finite bandwidth of the observations modifies the derived value of  $b$  by  $\lesssim 0.01$ .

Figs. 4 and 5 illustrate the effect of the size distribution on the polarization. In the computations of the phase matrix for these and all following figures the integration over particle radii was for the interval

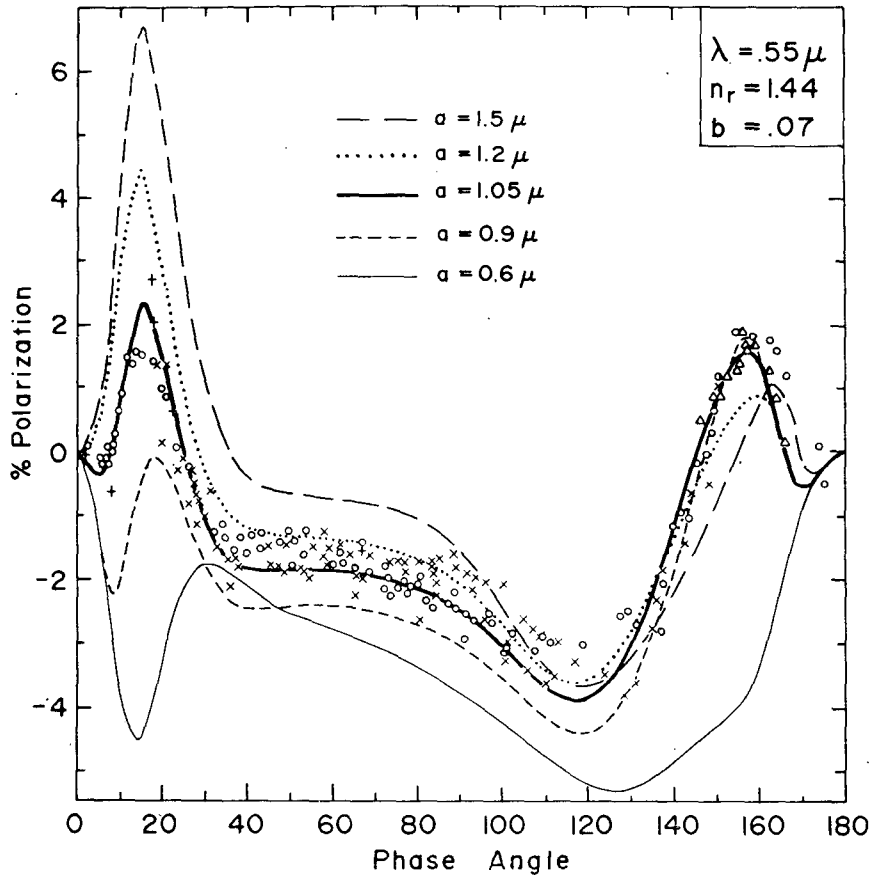


FIG. 4. Observations of the polarization of sunlight reflected by Venus in the visual wavelength region and theoretical computations for  $\lambda=0.55 \mu\text{m}$ . The  $\circ$ 's are wide-band visual observations by Lyot (1929) while the other observations are for an intermediate bandwidth filter centered at  $\lambda=0.55 \mu\text{m}$ ; the  $\times$ 's were obtained by Coffeen and Gehrels (1969), the  $+$ 's by Coffeen (cf. Dollfus and Coffeen, 1970), and the  $\Delta$ 's (which refer to the central part of the crescent) by Veverka (1971). The theoretical curves are all for a refractive index 1.44, the size distribution (8) with  $b=0.07$ , and a Rayleigh contribution  $f_R=0.045$ . The different curves show the influence of the effective radius on the polarization.

(0,  $5 \mu\text{m}$ ), which was sufficient that  $a=r_{\text{eff}}$  and  $b=v_{\text{eff}}$ . In Figs. 4 and 5 the refractive index is  $n_r=1.44$ , a value which provides good agreement with the observations. In Fig. 4  $b$  is held constant at 0.07 and  $a$  is allowed to vary from 0.6 to  $1.5 \mu\text{m}$ . For values of  $a$  outside this range the discrepancies with the observations increase. In Fig. 5  $a$  is held constant at  $1.05 \mu\text{m}$  and  $b$  is allowed to vary over a wide range. For  $b$  smaller than 0.02 or larger than 0.25 the discrepancies with the observations are still larger than the extremes illustrated.

In the theoretical curves the maximum in the polarization at phase angles  $\sim 20^\circ$  is the primary rainbow. The maximum at  $\sim 155^\circ$  is the feature of anomalous diffraction. If observations were only available in this one wavelength region, there would be no assurance that the features in the observations were actually due to a rainbow and anomalous diffraction. However, as is demonstrated below, large variations of these features occur with changing wavelength in precise agreement

with the theory for spheres, including a changeover toward Rayleigh scattering at wavelengths in the infrared. These wavelength variations are sufficient to demonstrate conclusively that our interpretation of the polarization features is valid.

Figs. 4 and 5 indicate that, if the refractive index is  $\sim 1.44$ , the polarization is consistent with the effective radius,  $\sim 1.05 \mu\text{m} \pm 0.1 \mu\text{m}$ , and the effective variance,  $\sim 0.07 \pm 0.02$ . Results at other wavelengths confirm these values, though the polarization at most other wavelengths is not as sensitive to the size distribution as it is at  $\lambda=0.55 \mu\text{m}$ . Note that the observations of Veverka (1971), obtained in search of a possible halo effect, are very useful for defining the anomalous diffraction feature and thus the width of the size distribution; Lyot (1929) also observed that feature but his observations were for a broader bandwidth.

Since the refractive index may, in principle, vary significantly with wavelength, it was necessary to

actually do a huge number of computations to try to investigate all possible values of  $a$ ,  $b$  and  $n_r(\lambda)$ . Fig. 6 shows theoretical results for the refractive indices, 1.33, 1.4 and 1.5 at  $\lambda=0.55 \mu\text{m}$ . For each value of  $n_r$  the value of  $a$  was chosen which yields the best agreement with the observations, the main criterion for agreement being the fit to the positive polarization maximum at phase angle  $\sim 15^\circ$ . It is possible to get the theoretical rainbow at the appropriate phase angle for a fairly wide range of  $n_r$ , because the angular location of the rainbow varies somewhat with  $a$  (cf. Fig. 2); thus, the larger values of  $n_r$  require a larger value of  $a$  to fit the observations. We used  $b=0.05$  in Fig. 6 so that the results can be related to the single scattering contour diagrams of Fig. 2. With a larger value of  $b$  the results for  $n_r=1.40$  can be brought into fair agreement with the observations. However, by making the assumption that  $n_r$  does not vary by more than  $\sim 0.01$  over several hundred angstroms in the visible region (cf. Section 4), we are able to conclude from the observations shown in Figs. 4-6 and the observations of Coffeen and Gehrels (1969) at  $\lambda=0.52$  and  $0.655 \mu\text{m}$ , Veverka at  $0.655 \mu\text{m}$  and Dollfus (cf. Dollfus and Coffeen, 1970) at  $\lambda=0.527$ ,  $0.593$  and  $0.617 \mu\text{m}$  that  $n_r(\lambda=0.55 \mu\text{m})=1.44 \pm 0.015$ .

#### b. Wavelength $\lambda=0.99 \mu\text{m}$

At wavelengths  $\sim 1 \mu\text{m}$  the observed polarization of Venus is negative at all phase angles, in contrast to the results for shorter wavelengths. The variation of the polarization with wavelength has a smooth transition as indicated by observations of Dollfus (1966), Coffeen

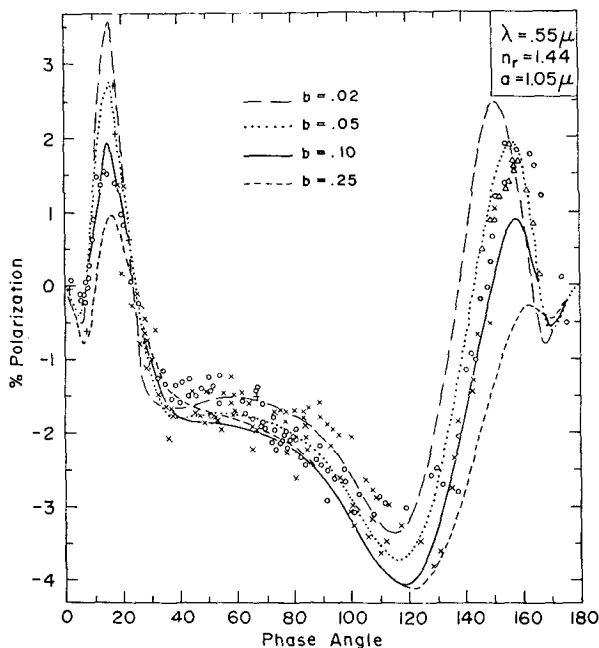


FIG. 5. As in Fig. 4 except that all of the theoretical curves are for  $a=1.05 \mu\text{m}$ , while the effective variance is allowed to range over the values 0.02 to 0.25.

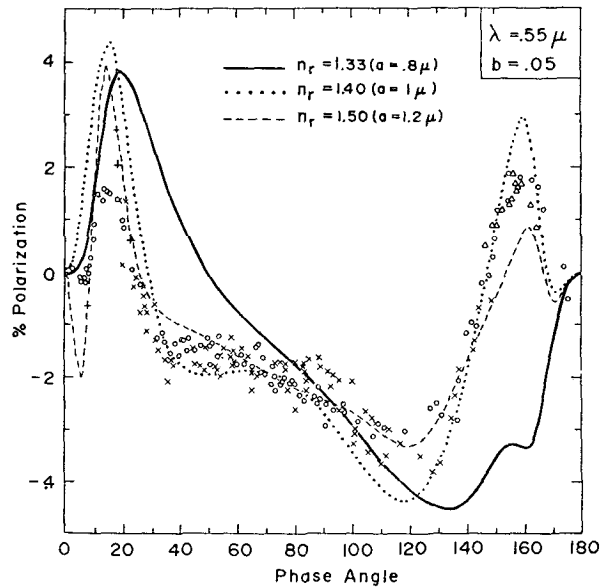


FIG. 6. Observations are the same as in Fig. 4. The theoretical curves are for three refractive indices with the effective particle radius chosen in each case to yield the best agreement with the observations. The size distribution is (8) with  $b=0.05$ . The Rayleigh contribution to the phase matrix is given by  $f_R=0.045$

and Gehrels (1969) and Dollfus and Coffeen (1970) at several wavelengths in the region  $0.34 \lesssim \lambda \lesssim 1 \mu\text{m}$ . The large difference in the polarization between visible and near-infrared wavelengths is a qualitative indication that the cloud particles must be on the order of the wavelength in size for this spectral region. If the particles were much larger (or smaller) than the wavelength the general shape of the polarization curve as a function of phase angle would not change so drastically with wavelength; this is illustrated in Figs. 2 and 3.

Single scattering computations for spheres qualitatively agree with the observations at  $\lambda=0.99 \mu\text{m}$  for refractive indices  $1.37 \lesssim n_r \lesssim 2$  [cf. Section 2 and Coffeen (1969)]. As illustrated by Figs. 2 and 3 the polarization for the relevant range of the effective size parameter is very sensitive to both the refractive index and the particle size. Thus, with accurate multiple scattering computations it is possible to find fairly narrow limits for these parameters.

Figs. 7 and 8 show observations for  $\lambda=0.99 \mu\text{m}$ , which is the wavelength in the near infrared with the greatest number of observations. The theoretical curves for these figures were computed with values of  $\bar{\omega}_0$  obtained from (10) with the spherical albedo of Venus taken as 0.90 (cf. Irvine, 1968). A Rayleigh contribution specified by  $f_R=0.045$  was included in the computations, but it had a negligible effect on the polarization. In Fig. 7 the theoretical curves are for different refractive indices, the particle size being chosen for each refractive index to yield the best agreement at all wavelengths. In choosing  $a$  special emphasis was placed on fitting the rainbow, which is present in the observed

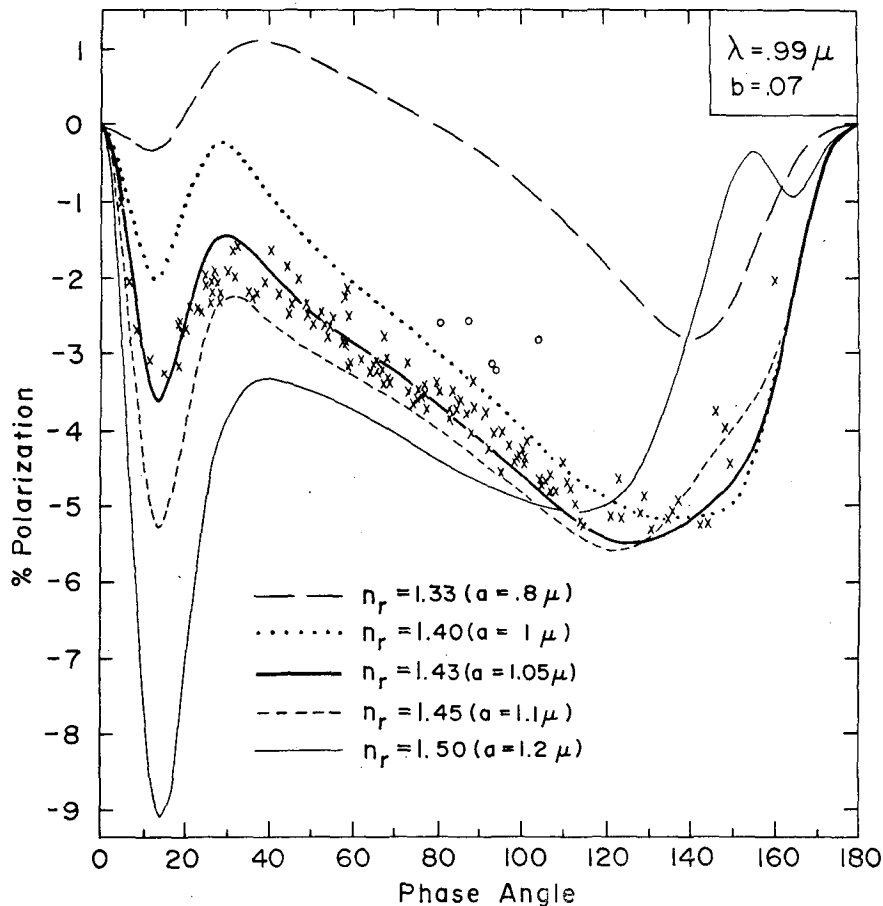


FIG. 7. Observations and theoretical computations of the polarization of sunlight reflected by Venus at  $\lambda = 0.99 \mu$ . The observations were made with an intermediate bandwidth filter, the  $\times$ 's being obtained by Coffeen and Gehrels (1969) in 1959-67 and by Coffeen (cf. Dollfus and Coffeen, 1970) from 1967 to March 1969, and the  $\circ$ 's being obtained by Coffeen (cf. Dollfus and Coffeen, 1970) in May-July, 1969. The theoretical curves are for spherical particles having the size distribution (8) with  $b = 0.07$ . The different theoretical curves are for various refractive indices, the effective particle radius being selected in each case to yield closest agreement with the observations for all wavelengths.

polarization for wavelengths  $\lesssim 1 \mu$ , and it was assumed that the dispersion of refractive indices between the visible region and  $\lambda = 0.99 \mu$  is  $\lesssim 0.04$  (cf. Section 4).

Fig. 7 illustrates the sensitivity of the polarization to the refractive index and indicates that  $n_r \approx 1.43$  provides the best fit. All of the curves in this figure are for  $b = 0.07$ ; however, as is shown in Fig. 3, the polarization at  $\lambda \approx 1 \mu$  (for  $a \approx 1 \mu$ ) is less sensitive to  $b$  than it is in the visible region. Furthermore, since the size distribution must be narrow enough for the anomalous diffraction feature to exist (at  $\lambda \approx 0.5-0.6 \mu$ ), there is little room for varying  $b$ .

Fig. 8 shows the sensitivity of the polarization to the effective particle radius  $a$ . A rather narrow range of acceptable sizes is indicated, with  $a \approx 1 \mu$ . For larger particles the rainbow becomes much too pronounced to agree with the observations. For smaller particles the theoretical polarization becomes less negative than that

observed, and it finally shifts to positive polarization at all phase angles as the Rayleigh region is approached.

The most recent observations of Coffeen (cf. Dollfus and Coffeen, 1970), shown as circles in Fig. 7 and 8, indicate a less negative polarization than the more numerous earlier observations of Coffeen and Gehrels (1969). Observations of Dollfus at  $\lambda = 0.95$  and  $1.05 \mu$  (cf. Dollfus and Coffeen, 1970) taken during some of the same years as the observations of Coffeen and Gehrels also tend to fall above the observations of Coffeen and Gehrels, although on the average they are not as far above as the circles in Figs. 7 and 8. The spread of the observations is thus somewhat greater than would be suggested by examination of only the early observations of Coffeen and Gehrels. However, the derived refractive index,  $n_r(\lambda = 0.99 \mu) = 1.43 \pm 0.015$ , was obtained with cognizance of all the observations.

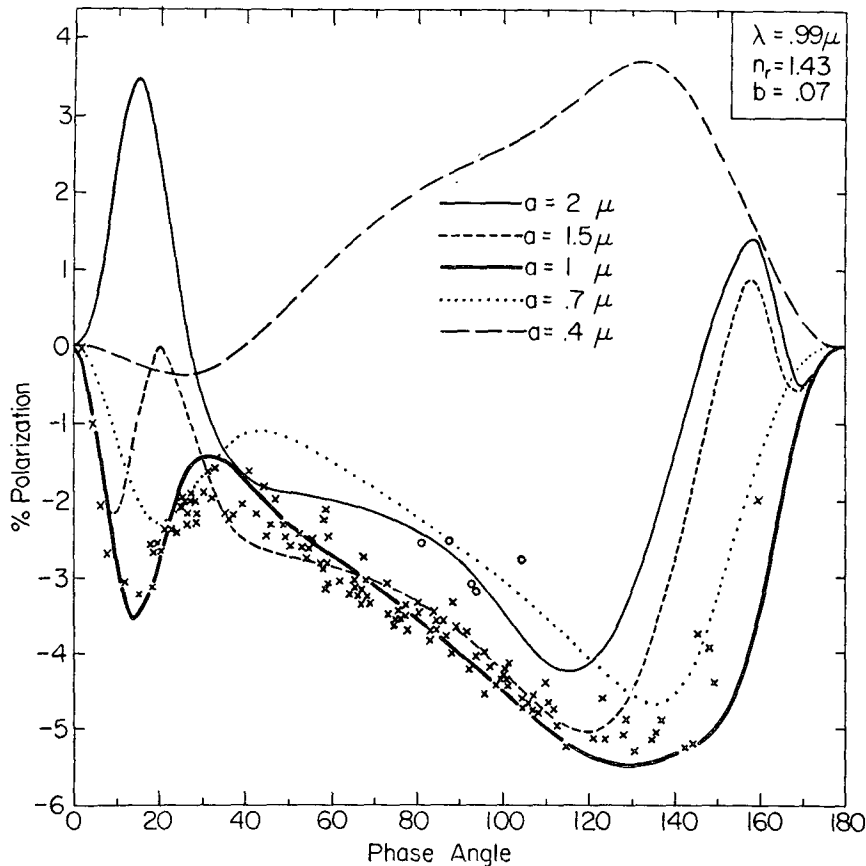


FIG. 8. The observations are the same as in Fig. 7. The theoretical curves are for spheres with refractive index  $n_r=1.43$ . The particle size distribution is (8) with  $b=0.07$  and with the different curves for five values of the effective radius  $a$ .

*c. Wavelength  $\lambda=0.365 \mu\text{m}$*

The polarization in the ultraviolet is less sensitive to the particle size distribution than it is in the visible or infrared regions. This can be understood from the single scattering contour diagrams (Figs. 2 and 3) along with knowledge of the fact that the observations at longer wavelengths require  $a$  to be  $\sim 1 \mu\text{m}$ . However, the UV observations are very useful for establishing the optical thickness of Rayleigh scatterers in or above the clouds. In addition the refractive index can be rather accurately obtained in this wavelength region since the rainbow has a sharp maximum.

The most extensive UV observations are for an intermediate bandpass centered at  $\lambda \approx 0.365 \mu\text{m}$ . In Figs. 9 and 10 the crosses are observations of Coffeen and Gehrels (1969) obtained from 1959 through 1967. The maximum polarization obtained in the rainbow during those years was  $\sim 7\%$  with the peak at phase angle  $\sim 17^\circ$ ; however, all of the points near the rainbow peak were measured during one apparition in 1965 except one point at phase angle  $21.1^\circ$  for which a polarization of  $5.6\%$  was obtained in 1967. The circles are observations obtained in 1967-69 by Coffeen (cf.

Dollfus and Coffeen, 1970). These show a maximum polarization  $\sim 10\%$  in the rainbow; two of the three points with polarization greater than  $9\%$  were obtained in January 1967 and the third during a different apparition in May 1968. The triangles are observations of Dollfus obtained in 1969 (cf. Dollfus and Coffeen, 1970); these measurements refer to the central portion of the crescent. We include these local observations in our figure because there are no published disk-integrated observations at large phase angles for  $\lambda \approx 0.365 \mu\text{m}$ . Below we illustrate that at large phase angles the theoretical polarization for this spot on the planet differs little from that for the light integrated over the planet.

The calculations in Fig. 9 are for the size distribution (8), with  $a=1.05 \mu\text{m}$  and  $b=0.07$  being selected to obtain good agreement with the polarization observations at all wavelengths. The refractive index,  $n_r=1.45$ , was chosen to give a good fit to the location of the rainbow for  $\lambda=0.365 \mu\text{m}$ . Fig. 9 thus illustrates the effect of Rayleigh scattering on the polarization in the ultraviolet. As described above,  $f_R$  is the ratio of the Rayleigh scattering coefficient to the cloud particle scattering

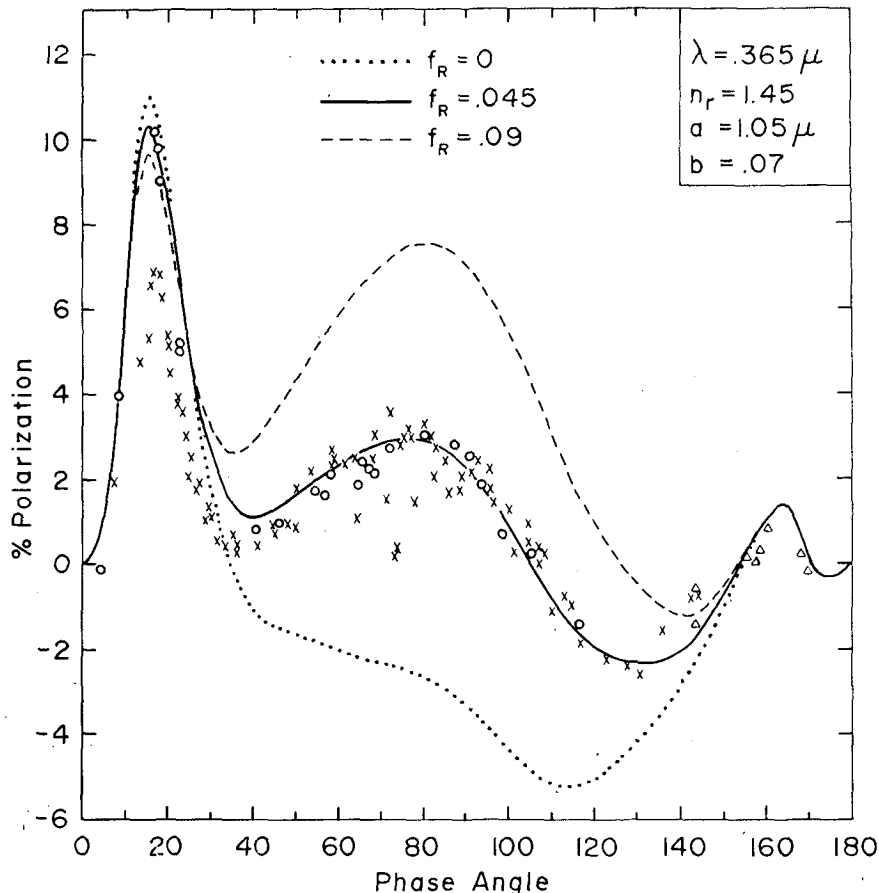


FIG. 9. Observations and theoretical calculations of the polarization of sunlight reflected by Venus at  $\lambda=0.365 \mu\text{m}$ . The observations were made with intermediate bandwidth filters centered at  $\lambda=0.365 \mu\text{m}$ , the X's being obtained by Coffeen and Gehrels (1969) in 1959-67, the O's by Coffeen in 1967-69 (cf. Dollfus and Coffeen, 1970), and the  $\Delta$ 's by Dollfus in 1969 (cf. Dollfus and Coffeen, 1970). The observations of Coffeen and Gehrels refer to the entire visible planetary disk, while those of Dollfus refer to an area on the disk midway between limb and terminator. The theoretical curves are the results after integration over the visible disk. They are for a homogeneous atmosphere containing spherical particles of the size distribution (8) with  $a=1.05 \mu\text{m}$  and  $b=0.07$ . The refractive index of the particles is 1.45. The three theoretical curves are for different Rayleigh contributions to the phase matrix.

coefficient. Fig. 9 indicates that the best value of  $f_R$  for a homogeneous atmosphere is  $f_R \approx 0.045$ . Using the relation

$$p_1 \approx 1.16 f_R [p_1 \text{ in bars}], \quad (14)$$

where  $p_1$  is the pressure level at cloud optical depth unity (see the Appendix),<sup>5</sup> we find that the atmospheric pressure at cloud optical depth unity is  $\sim 50$  mb.

This derived pressure level depends significantly on our assumption of a homogeneous atmosphere. However, even if the atmosphere of Venus is vertically inhomogeneous (as is probable) the cloud optical depth unity must nevertheless be at a pressure on the order of 50 mb. This is a result of the fact that, roughly stated, the polarization arises from optical depths

<sup>5</sup> We also show in the Appendix that the effect of molecular anisotropy on this relation is negligible.

between zero and unity. It is unlikely that the error in the pressure at cloud optical depth unity is more than  $\sim 25$  mb. However, this quantity and the vertical distribution of particles should be more thoroughly investigated by means of computations for an inhomogeneous atmosphere and comparisons to observations of high spatial resolution.

Fig. 10 illustrates the sensitivity of the polarization in the ultraviolet to the refractive index. For each of the three refractive indices, 1.33, 1.4 and 1.5, that value of  $a$  is shown which yields best agreement with the observations for all wavelengths; in choosing  $a$  it was assumed that the dispersion of the refractive index between the UV and visible regions is  $\lesssim 0.04$ . Parameters  $b=0.07$  and  $f_R=0.045$  are the same for all three curves. For  $n_r=1.40$  the agreement with observations at phase angles  $\sim 80^\circ$  can be improved by choosing  $f_R=0.035$ ,

while for  $n_r=1.50$  the agreement can be improved at phase angles  $\sim 160^\circ$  by choosing  $b=0.10$ . However, such variations of  $f_R$  and  $b$  do not significantly affect the rainbow, which is the primary determinant of the refractive index at this wavelength.

Figs. 9 and 10 show that the refractive index for  $\lambda=0.365 \mu\text{m}$  is  $\sim 1.45$ . The value  $n_r=1.46$  fits at least as well as 1.45, the observations on the sides of the rainbow being approximately equidistant from the calculated curve for  $n_r=1.46$ . The movement of the rainbow for small changes of  $n_r$  can be estimated by interpolating between the results in Figs. 9 and 10; also, Hansen and Arking (1971) and Coffeen and Hansen (1973) have published computations for  $n_r=1.46$ . As is indicated below, the best agreement at  $\lambda=0.34 \mu\text{m}$  appears to occur with  $n_r$  between 1.46 and 1.47. Taking this into account we conclude that  $n_r(\lambda=0.365 \mu\text{m})=1.46 \pm 0.015$ .

The UV observations in the rainbow region during 1965 show a polarization smaller than that measured in two later apparitions and smaller than that obtained theoretically. Dollfus and Coffeen (1970) discussed the possibility of a "red leak" in the observing systems, which would have decreased the polarization, but they concluded that the time variation of the polarization was probably real. The UV polarization was also lower at most other phase angles during the 1965 apparition (cf. Fig. 3 of Dollfus and Coffeen, 1970), and in general the polarization is more variable in the ultraviolet than

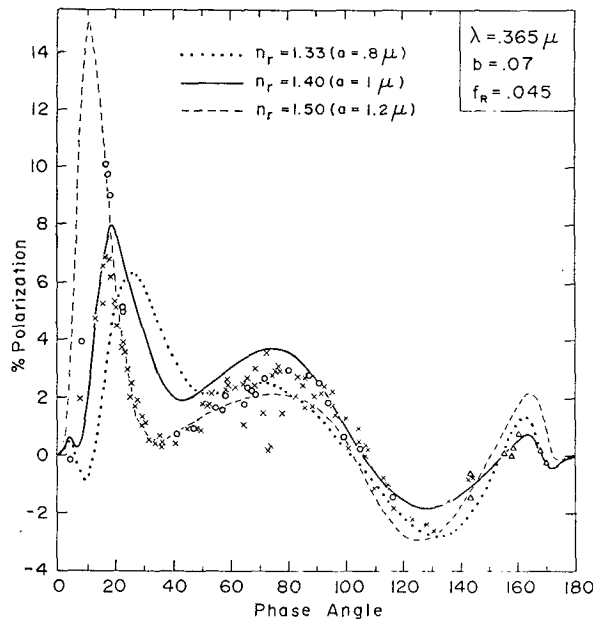


FIG. 10. The observations are the same as in Fig. 9. The theoretical curves are for a homogeneous atmosphere containing spherical particles of the size distribution (8) with  $b=0.07$ . The Rayleigh contribution to the phase matrix is specified by  $f_R=0.045$ . The different theoretical curves are for different refractive indices, in each case with  $a$  chosen to yield the best agreement at all wavelengths.

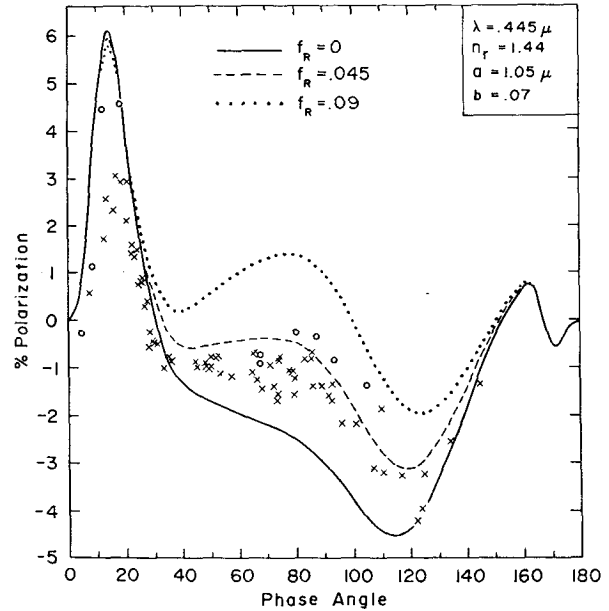


FIG. 11. Observations and theoretical calculations of the polarization of sunlight reflected by Venus at  $\lambda=0.445 \mu\text{m}$ . The observations were made with intermediate bandwidth filters, the X's being obtained by Coffeen and Gehrels (1969) in 1959-67 and the O's by Coffeen in 1967-69 (cf. Dollfus and Coffeen, 1970). The theoretical curves are for a homogeneous atmosphere containing spherical particles of the size distribution (8) with  $a=1.05 \mu\text{m}$  and  $b=0.07$ . The refractive index of the particles is 1.45. The three theoretical curves are for different Rayleigh contributions to the phase matrix.

at longer wavelengths (cf. Fig. 17 of Coffeen and Hansen, 1973). It seems likely that the variability of the UV polarization is related to the variable UV markings on the planet (Boyer and Camichel, 1961; Dollfus, 1968; Boyer and Guerin, 1969; Scott and Reese, 1972).

Variations in the polarization could arise, for example, from changes in the cloud height, the number density of cloud particles, the UV cloud albedo, or the fraction of the planet covered by high clouds. It is probable that the effects of both vertical and horizontal atmospheric inhomogeneities are more significant in the ultraviolet than at longer wavelengths. Indeed, UV polarization and intensity measurements with high spatial and temporal resolution, e.g., from an orbiting spacecraft, would be ideally suited for investigating the atmospheric structure.

*d. Other wavelengths*

The three wavelengths for which results of calculations are presented above are those with the greatest number of observations, and they practically span the region (0.34-1  $\mu\text{m}$ ) in which measurements have been concentrated. However, we have examined all of the observations mentioned in Section 1 and compared them with theoretical computations. Below we give a

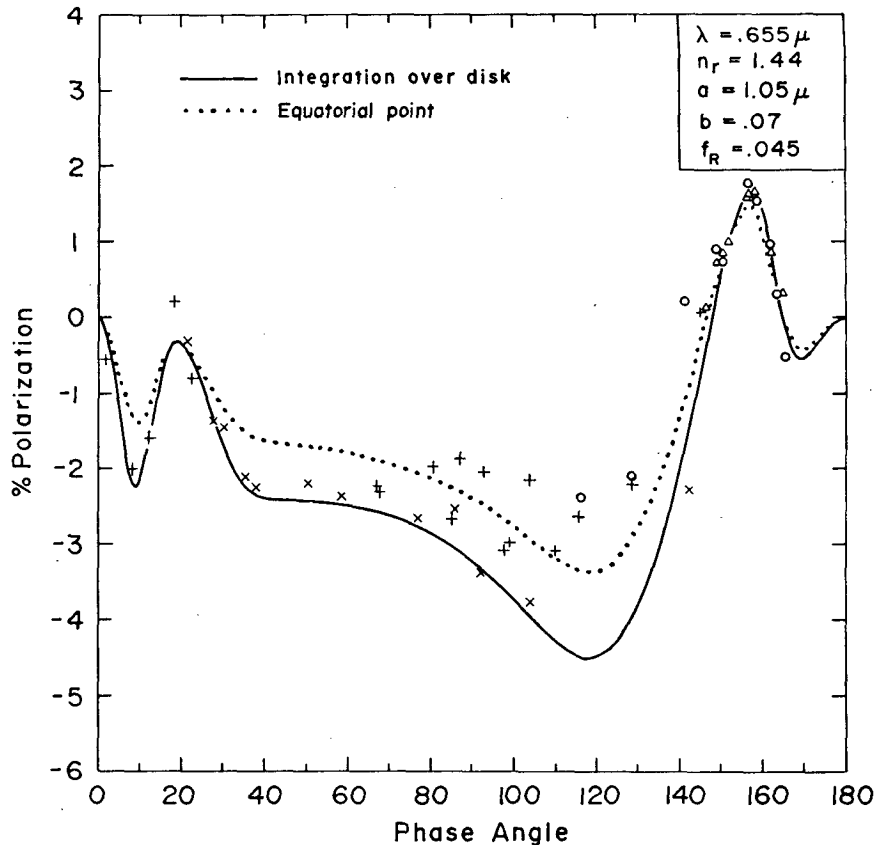


FIG. 12. Observations and theoretical calculations of the polarization of sunlight reflected by Venus at  $\lambda = 0.655 \mu$ . The observations were made with intermediate bandwidth filters. The  $\times$ 's (Coffeen and Gehrels, 1969) and  $+$ 's (Dollfus and Coffeen, 1970) refer to the entire visible planetary disk. The  $\circ$ 's (Dollfus and Coffeen, 1970) and  $\Delta$ 's (Veverka, 1971) refer to the central portion of the crescent. The theoretical computations are for a homogeneous atmosphere containing spherical particles of the size distribution (8) with  $a = 1.05 \mu$  and  $b = 0.07$ . The refractive index of the particles is  $n_r = 1.44$  and the Rayleigh contribution is  $f_R = 0.045$ . The solid curve refers to light integrated over the planetary disk and the dotted curve refers to the point on the equator with  $\theta_0 = \theta = \rho/2$ .

summary of results at other wavelengths. Except where indicated otherwise, the wavelengths mentioned below refer to intermediate passband filters of Coffeen and Gehrels. The observations of Dollfus, which are in essentially the same region as the observations of Coffeen and Gehrels, are in rather good agreement with those of Coffeen and Gehrels (cf. Dollfus and Coffeen, 1970).

At  $\lambda = 0.34 \mu$  the observations are similar to those at  $\lambda = 0.365 \mu$ . Under the assumption that  $a \approx 1.05 \mu$ ,  $b \approx 0.07$ , the best fit to the rainbow is for  $n_r = 1.46$  or  $1.47$ . The observations at intermediate phase angles are fit best with a Rayleigh scattering contribution  $f_R \approx 0.04$ .

At  $\lambda = 0.4 \mu$  the observations are entirely those of Dollfus (cf. Dollfus and Coffeen, 1970). Calculations with  $a = 1.05 \mu$ ,  $b = 0.07$  and  $n_r = 1.45$  are in good agreement with the observations. All of the observations for phase angles  $35^\circ$ – $110^\circ$  were obtained during one

apparition (1967). For those observations the best fit for the contribution of Rayleigh scattering is  $f_R \approx 0.05$ .

Observations for  $\lambda = 0.445 \mu$  are shown in Fig. 11. The crosses were obtained by Coffeen and Gehrels (1969) in 1959–67; the circles were obtained by Coffeen in 1967–69 (cf. Dollfus and Coffeen, 1970). Most of the points in the rainbow region were measured during one apparition in 1965; of the two points with polarization exceeding 4%, one was obtained in 1967 and the other during a different apparition in 1968. The theoretical curves in Fig. 11 are for  $n_r = 1.44$ ,  $a = 1.05 \mu$  and  $b = 0.07$ . These were computed with  $\tilde{\omega}_0$  obtained from (10) for an assumed spherical albedo of Venus of 0.75 (cf. Irvine, 1968). The theoretical curves illustrate that a Rayleigh contribution  $f_R \approx 0.045$  fits the 1967–69 observations, while  $f_R \approx 0.035$  is a better fit to the older observations. Dollfus' observations at  $\lambda = 0.44 \mu$  (cf. Dollfus and Coffeen, 1970) are fit best by  $f_R \approx 0.045$ . The rainbow at  $\lambda = 0.445 \mu$  can be fit about equally well for any refractive index in the range 1.43–1.46.

At  $\lambda=0.52 \mu\text{m}$  the observations are similar to those at  $\lambda=0.55 \mu\text{m}$ . Several measurements are available in the region of anomalous diffraction. These are useful for establishing the width of the size distribution and they are in agreement with  $b \approx 0.07$ .

Observations for  $\lambda=0.655 \mu\text{m}$  are shown in Fig. 12. Those obtained by Coffeen and Gehrels (1969) in 1966-67 and those by Coffeen in 1967-1969 (cf. Dollfus and Coffeen, 1970) refer to the entire visible planetary disk; those obtained by Coffeen in 1969 (cf. Dollfus and Coffeen, 1970) and Veverka (1971) in 1969 refer to the central portion of the crescent. The theoretical curves in Fig. 12 are for  $n_r=1.44$ ,  $a=1.05 \mu\text{m}$ ,  $b=0.07$  and  $f_R=0.045$ . These were computed with  $\bar{\omega}_0$  obtained from (10) with the spherical albedo of Venus taken as 0.95 (cf. Irvine, 1968). The solid curve is the theoretical polarization for the entire visible planetary disk, while the dotted curve is for the point on the equator with  $\theta_0=\theta=\rho/2$ , where  $\theta_0$  and  $\theta$  are the zenith angles for the incident and emergent light, respectively, and  $\rho$  is the phase angle. The absolute value of the polarization is generally higher for the disk-integrated light than for the light from the equatorial midpoint. This is easy to understand since a significant fraction of the disk-integrated light is from the limb or terminator, where single scattering dominates and the polarization is high. Thus, the polarization for the area observed about the equator should also be somewhat less than that for the entire visible planetary disk. The available observations at  $\lambda=0.655 \mu\text{m}$  are primarily useful for determining the width of the size distribution; they indicate that  $b \approx 0.07$ .

At  $\lambda=0.685 \mu\text{m}$  and  $\lambda=0.74 \mu\text{m}$  the observations fit calculations for  $n_r=1.43$  or  $1.44$ ,  $a=1.05 \mu\text{m}$ ,  $b=0.07$  and  $f_R=0.045$ . There are no observed points in the region of anomalous diffraction and only a few at phase angles less than  $20^\circ$ .

At  $\lambda=0.875 \mu\text{m}$  the observations are in good agreement with calculations for  $n_r=1.43$ ,  $a=1.05 \mu\text{m}$ ,  $b=0.07$  and  $f_R=0.045$ .

A few observations have been made in the infrared between wavelengths 1.25 and  $3.6 \mu\text{m}$ . Forbes (1971) has made several observations at  $\lambda=1.25$ , 1.65, 2.25 and  $3.6 \mu\text{m}$ . These observations contain large fluctuations, sometimes varying by 2 or 3% polarization in a few days. Kuiper (1957) made measurements at wavelength  $2 \mu\text{m}$ , reporting results for the phase angle  $80^\circ$  and for several phase angles in the range  $141^\circ$ - $162^\circ$ . The infrared observations are thus too sparse and uncertain to allow a precise refractive index or other detailed information to be derived. However, it is significant that the observations yield negative polarization at all observed phase angles for  $\lambda=1.25$ , 1.65 and  $2 \mu\text{m}$ , but primarily positive polarization for  $\lambda=2.2 \mu\text{m}$  and only positive polarization for  $\lambda=3.6 \mu\text{m}$ . The contour diagrams in Figs. 2 and 3 show that this is just the behavior expected of cloud particles with  $a \approx 1 \mu\text{m}$ , and thus our basic interpretation of the polarization is

reconfirmed in a region of the spectrum where the polarization has an entirely different nature than that in the visual region.

#### 4. Refractive indices

We have shown that the real refractive index of the Venus cloud particles is  $1.44 \pm 0.015$  at  $\lambda=0.55 \mu\text{m}$ , and that the refractive index varies from  $\sim 1.46$  at  $\lambda=0.365 \mu\text{m}$  to  $\sim 1.43$  at  $\lambda=0.99 \mu\text{m}$ . The main value of this information is the precise criterion it provides for the cloud particle composition. Different materials which have been proposed for the composition of the Venus clouds can be examined to see if they have the appropriate  $n_r(\lambda)$ ; to be in agreement with the polarization of Venus the material must also have a negligible absorptivity in the visual region and it must form spherical particles at the conditions in the Venus cloudtops.

##### a. Interpolation formulas

The refractive indices of most materials vary significantly with temperature and wavelength, but in many cases laboratory measurements of  $n_r$  exist for at most a few values of  $T$  and  $\lambda$ . Thus, it is important to have a method to interpolate and/or extrapolate from a few measured points. For this purpose we use two formulas of classical physics, given, for example, by Born and Wolf (1965). These formulas are applicable to isotropic substances in a spectral region with negligible absorptivity, provided also that the frequency is high enough ( $\gtrsim 10^{11}$  Hz) to ensure that the molecules behave as nonpolar molecules.

The formula we use for the temperature dependence of the refractive index is the Lorentz-Lorenz equation written in the form

$$\frac{n_r^2 - 1}{n_r^2 + 2} = \frac{M}{W} \rho(T), \quad (15)$$

where  $M$  is the molar refractivity of the material,  $W$  the molecular weight, and  $\rho(T)$  the density at temperature  $T$ . If the molecules keep their identity,  $M$  is nearly independent of temperature and density for most materials. For example, a typical variation of  $M$  is an increase of 0.01% per degree Kelvin (cf. Batsanov, 1961); it has also been experimentally verified at 20C for sodium light that  $dn_r/dT$  for water and  $\text{CS}_2$  is almost entirely accounted for by the change in density with temperature (cf. Jaffé, 1928). Thus (15) gives the temperature dependence of  $n_r$  at any specific wavelength, provided reliable data are available for  $\rho(T)$ .

We also need a formula for the dispersion, i.e., for the wavelength dependence of the refractive index. The refractive index of a material at a particular density satisfies

$$\frac{n_r^2 - 1}{n_r^2 + 2} = \sum_i \frac{s_i}{\nu^2 - \nu_i^2}, \quad (16)$$

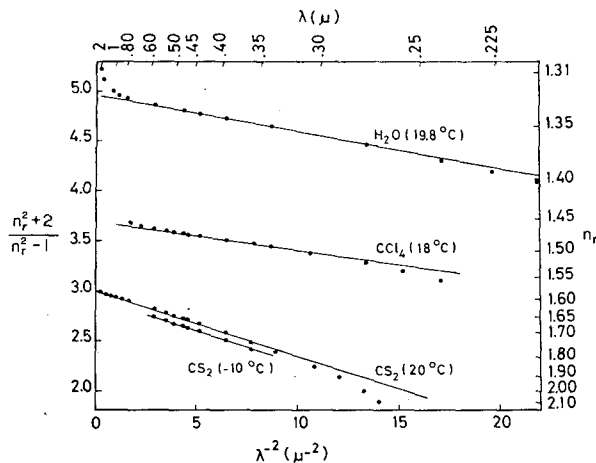


FIG. 13. Refractive indices of several liquids as a function of wavelength. Experimental values are represented by dots. The data for water were taken from Jaffé (1928) and the data for  $\text{CCl}_4$  and  $\text{CS}_2$  were derived from tables of Hellwege (1962). The straight lines are eyeball fits to the near-linear domains.

where  $\nu$  is the frequency and each  $\nu_i$  is a resonance frequency corresponding to a "strength"  $s_i$ . Damping is neglected in (16); this is equivalent to the assumption that absorption is negligible, as is true at frequencies far from any  $\nu_i$ . Thus, the formula is particularly useful in the visible part of the spectrum for substances transparent to the eye. The resonance frequencies for such materials fall in the ultraviolet and in the infrared, and the refractive index for visible light is primarily determined by the UV resonances.

We would like an interpolation formula which has only a few parameters, but which is still accurate enough for our purposes. Thus, we replace (16) with the simple formula

$$\frac{n_r^2 - 1}{n_r^2 + 2} = \frac{a}{\nu^2 - \nu_a^2} \quad (17)$$

where the two parameters  $a$  and  $\nu_a$  can be determined from values of  $n_r$  measured for a given temperature at two or more wavelengths. Eq. (17) can be thought of as lumping all resonance frequencies into an average resonance frequency  $\nu_a$ . Although many empirical dispersion formulas have been published, we have not found the above formula used in the literature as a simple interpolation tool. If the denominator on the left-hand side of (17) is omitted, we obtain a one-term Sellmeier dispersion formula which has often been used (cf. Born and Wolf, 1965, Sec. 2.3). However, one advantage of (17) is that, according to (15),  $a$  is simply proportional to the density.

We have used laboratory measurements of  $n_r$  to check the accuracy of (17) and to demonstrate the significance of deviations from that equation. We rewrite (17) in the form

$$\frac{n_r^2 + 2}{n_r^2 - 1} = \frac{c^2}{a} \left( \frac{1}{\lambda^2} - \frac{1}{\lambda_a^2} \right), \quad (18)$$

where  $c$  is the speed of light, and plot the measured values as  $(n_r^2 + 2)/(n_r^2 - 1)$  vs  $1/\lambda^2$ . We have made such plots for a number of colorless liquids at various temperatures. Fig. 13 shows results for water,  $\text{CCl}_4$  and  $\text{CS}_2$ . In each case we find that the linear dependence implied by (18) is indeed a good approximation over a wide range of wavelength. To bring this out more clearly we have included in Fig. 13 straight lines which are eyeball fits to the near-linear domains. We conclude that for colorless liquids  $(n_r^2 + 2)/(n_r^2 - 1)$  is approximately linearly dependent on  $1/\lambda^2$  for visible wavelengths.

The deviations from straight lines in Fig. 13 arise from strong absorption in the ultraviolet and infrared. For water the increase in  $(n_r^2 + 2)/(n_r^2 - 1)$  for  $\lambda \gtrsim 1 \mu\text{m}$  is a result of the fundamental vibration-rotation band in the  $\lambda \approx 3 \mu\text{m}$  region. As shown by the data of Irvine and Pollack (1968), the absorptivity of water has a strong maximum at  $\lambda \approx 2.95 \mu\text{m}$  with a corresponding minimum in  $n_r$  at  $\lambda \approx 2.75 \mu\text{m}$ . At the other end of the spectrum,  $(n_r^2 + 2)/(n_r^2 - 1)$  for  $\text{CS}_2$  bends below the straight line, indicating appreciable absorption in the near-ultraviolet.

Fig. 13 also illustrates a check on the temperature dependence of  $n_r$ . According to Eq. (15),  $(n_r^2 + 2)/(n_r^2 - 1)$  should shift by some constant factor when the temperature is changed. This is demonstrated by data for  $\text{CS}_2$ . The ratio of the experimental values for  $(n_r^2 + 2)/(n_r^2 - 1)$  at  $-10^\circ\text{C}$  and  $+20^\circ\text{C}$  varies only from 0.97149 at  $\lambda = 0.3612 \mu\text{m}$  to 0.97087 at  $\lambda = 0.5893 \mu\text{m}$ .

#### b. Application to Venus

The open circles in Fig. 14 are the refractive indices deduced from the polarization of Venus, with the "error bars" representing the maximum uncertainty in  $n_r$ . The three open circles happen to fall almost exactly on a straight line, as indicated by a heavy line. It is gratifying that the dispersion obtained for the Venus cloud particles is "normal," i.e., of the same sign and small magnitude as for colorless liquids. This result is consistent with the observed high albedo of Venus from  $\lambda \approx 0.35 \mu\text{m}$  to  $\lambda \approx 2 \mu\text{m}$ .

Hansen and Arking (1971) found that none of the materials proposed for the Venus clouds prior to 1970 were in good agreement with the polarization. However, carbon suboxide ( $\text{C}_3\text{O}_2$ ) and an aqueous solution of hydrochloric acid ( $\text{HCl} \cdot n\text{H}_2\text{O}$ ) are sufficiently near the required  $n_r$  to warrant examination. In Fig. 14 the dots for  $\text{C}_3\text{O}_2$  at 273K represent measurements of Diels and Blumberg (1908) for the Fraunhofer C, D and G lines ( $\lambda = 0.656, 0.589$  and  $0.434 \mu\text{m}$ , respectively). The point for  $T = 261\text{K}$ ,  $\lambda = 0.589 \mu\text{m}$  was also measured by Diels and Blumberg; we obtained the other points for that temperature from the assumption that the ratio of  $(n_r^2 + 2)/(n_r^2 - 1)$  for the two temperatures is the same at all wavelengths. Observations of several types indicate that the temperature of the Venus cloud tops

is  $\sim 220$ – $250$ K: absorption bands in reflected sunlight suggest  $T \approx 250$ K (Young, 1972); thermal radiation in the  $8$ – $13\mu$  m window indicates  $T \approx 220$ – $250$ K (cf. Hanel *et al.*, 1968); the radiometric albedo of  $77\%$  (Irvine, 1968) corresponds to an effective temperature  $\sim 237$ K; atmospheric models based on Mariner 5 measurements yield a temperature  $\sim 225$ K at the  $50$ -mb level (Fjeldbo *et al.*, 1971). Thus, we conclude that the clouds of Venus are not  $C_3O_2$ .

Lewis (1971, 1972) has suggested that the clouds of Venus may be an aqueous solution of hydrochloric acid with  $25$ – $30\%$  HCl by weight at a temperature near  $200$ K. In Fig. 14 we have plotted the refractive index for a  $27.6\%$  HCl solution at  $20$ C; the data were obtained by interpolating between measurements of Howell (cited by Timmermans, 1960) for proximate concentrations. In addition, we have used density determinations of Garret and Woodruff (1951) and the Lorentz-Lorenz formula (15) to reduce the values of  $(n_r^2+2)/(n_r^2-1)$  to  $200$ K; a similar procedure has been used by Lewis. Fig. 14 illustrates that this solution of HCl is not compatible with the refractive index of the Venus cloud particles, especially since the temperature in the Venus clouds is probably greater than  $200$ K. A stronger HCl concentration might have the appropriate refractive index, but such strong concentrations are apparently not consistent with observed abundances of gaseous HCl and  $H_2O$  (Young, 1973).

Recently, Sill (1972) and Young (1973) have independently suggested that the cloud particles on Venus may be a strong aqueous solution of sulfuric acid [cf. also Young and Young (1973) and Young (1974)]. Young proposes a freezing solution which he specifies as  $75.9\%$   $H_2SO_4$  by weight at  $250$ K; Sill suggests an  $86\%$  concentration at  $T=235$ K. We have derived values of  $n_r$  at several wavelengths for a  $75.9\%$  solution at  $T=15$ C by interpolation between measurements of Veley and Mauley (cf. Timmermans, 1960) for proximate concentrations. The resulting values for  $(n_r^2+2)/(n_r^2-1)$  are shown as dots in Fig. 14. Young (1973) has given the value  $n_r(\lambda=0.589\mu\text{m})=1.44193$  for  $T=250$ K which he obtained by extrapolating density measurements for higher temperatures and by using the Lorentz-Lorenz relation. From this value and the assumption of a constant scale factor for  $(n_r^2+2)/(n_r^2-1)$ , we obtained  $n_r(\lambda)$  at that temperature. The result is in excellent agreement with the refractive index of the Venus cloud particles. Somewhat different concentrations and temperatures would also be compatible with the polarization, e.g., concentrations  $\gtrsim 75\%$  may have the required refractive index if they are supercooled.

None of the other materials which have been suggested in the literature as composing the Venus clouds and clearly specified are compatible with the polarization. We mention here two substances for which there have been claims of conclusive identification with the visible clouds of Venus:  $H_2O$  and hydrated  $FeCl_2$ .

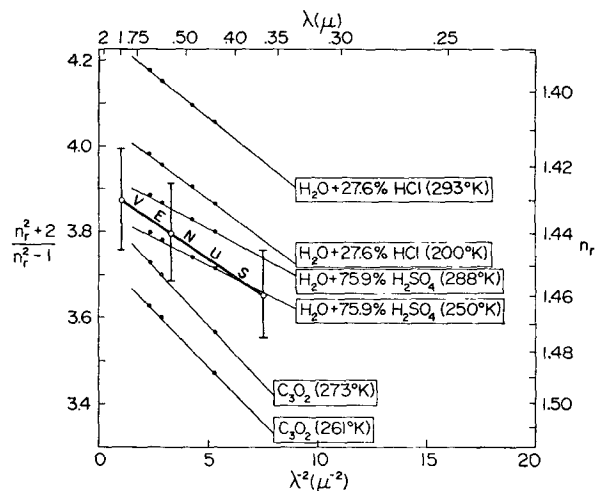


FIG. 14. Refractive indices of the Venus cloud particles (open circles) deduced from the polarization. The error bars represent the maximum uncertainty, not a probable error. The experimental values (dots) for the indicated liquids are based on laboratory measurements and, in some cases, interpolation formulas, as explained in the text.

Water has a refractive index much smaller than that of the particles in the visible Venus clouds, as illustrated in Fig. 13. Freezing the water only increases the disparity with the polarization of Venus, because ice tends to form nonspherical crystals. Iron chloride has a refractive index much larger than that of the particles in the visible Venus clouds (Kuiper, 1969); in addition, iron chloride would probably be in the form of platy crystals at the conditions in the Venus clouds.

## 5. Conclusions

Analysis of the polarization of sunlight reflected by Venus leads to several specific conclusions on the nature of the visible clouds of Venus. This information is remarkable because of the precision and certainty with which it defines physical properties of the cloud particles. These properties are:

**REFRACTIVE INDEX AND DISPERSION.** The index of refraction of the particles in the visible clouds is  $n_r=1.44\pm 0.015$  at  $\lambda=0.55\mu\text{m}$ . The indicated uncertainty refers to the limits for acceptable values, not to a probable error. The refractive index has a normal dispersion, decreasing from  $1.46\pm 0.015$  at  $\lambda=0.365\mu\text{m}$  to  $1.43\pm 0.015$  at  $\lambda=0.99\mu\text{m}$ .

**PARTICLE SHAPE.** The particles in the visible clouds of Venus are spherical. There is a clear signature of the particle shape in the polarization as a function of scattering angle, and its interpretation is confirmed by the variation of the polarization with wavelength.

**SIZE DISTRIBUTION (MEAN SIZE AND VARIANCE).** The effective radius [cf. (6)] for the size distribution of the cloud particles is  $1.05\pm 0.10\mu\text{m}$  and the effective variance [cf. (7)] is  $0.07\pm 0.02$ . By terrestrial standards

this is a narrow size distribution. Under the assumption that the shape of the Venus size distribution resembles the distribution (8) [cf. Fig. 1], the above values correspond to a mode radius  $r_m = 0.83 \pm 0.08 \mu\text{m}$  and a standard deviation  $\sigma = 0.26 \mu\text{m}$ .

**PRESSURE AT THE CLOUD TOPS.** The atmospheric pressure at cloud optical depth unity is  $\sim 50$  mb. This value, unlike the properties above, depends on the model which we use for the vertical distribution of particles and gas. We estimate the uncertainty in this number to be  $\pm 25$  mb.

There is, in addition, an important corollary to the derived physical properties of the cloud particles: *the particle size, shape and refractive index are very uniform over most of the illuminated part of the planet.* This refers to the visible clouds down to an optical depth at least  $\sim 1$ . It has been demonstrated (e.g., Hansen and Hovenier, 1971) that the polarization is primarily due to single-scattered photons, with qualitatively similar but smaller contributions from photons scattered two or three times. Thus, if there is more than one type of particle present, due to a mixture or layering of particles at a given location or to variations across the planet, each type of particle contributes to the polarization essentially according to its share of the "single" scattered light. If there were two types of spherical particles, differing say in refractive index, the polarization of each would appear in the observations; for example, in the case of transparent spheres larger than the wavelength, the rainbows for both types of particles would be present in the polarization. However, all of the features observed in the polarization of Venus are due to the particles described above. It is possible that a small fraction of the planet is covered by particles of another type, especially if those particles are of an irregular shape such that their polarization is rather featureless. The polar regions of Venus, for example, contribute only a small fraction of the light from the total disk, so the cloud properties could be quite different there. Also, the deviations which sometimes exist between the observations in the ultraviolet and the theoretical polarization could be due to a variation of cloud particle properties over part of the planet.

It is surprising that the particle size is so uniform over the planet. The value derived for the effective variance of the size distribution refers to an average size distribution over the illuminated part of the planetary disk down to optical depth  $\sim 1$ . Such a uniform particle size is uncharacteristic of terrestrial clouds in which the effective radius varies from a few micrometers to about  $100 \mu\text{m}$ , and the effective variance for individual clouds varies from  $\sim 0.05$  to  $\sim 0.40$ . However, the size distribution of particles in the stratospheric aerosol (Junge) layer on Earth has been measured by Mossop (1965) and Friend (1966) who both found  $v_{\text{eff}} \approx 0.06-0.08$ . Since the Junge layer exists at the pressure level  $\sim 50$  mb, this suggests a close analogy with the atmospheric

particles on Venus, as we have previously pointed out (cf. Hunten, 1971).

The above properties can be used for additional inferences about the nature of the Venus atmosphere. The most important of these concerns the *cloud composition*. Of all the materials proposed in the literature for the Venus clouds and clearly specified, the only material in agreement with the polarization is a concentrated solution of sulfuric acid. The similarities mentioned above between the Venus particles and the Junge layer on Earth, together with the fact that the Junge layer contains a large fraction of sulfuric acid (Rosen, 1971; Lazrus *et al.*, 1971; Toon and Pollack, 1973) support the conclusion that the composition of the cloud particles is sulfuric acid. Since the particles in the Junge layer are smaller [ $r_{\text{eff}} = 0.3-0.4 \mu\text{m}$ ; Friend (1966)] and have a much smaller optical thickness [ $\sim 2 \times 10^{-2}$ ; Elterman *et al.* (1973)], the mass of particles above unit area on Venus must be at least a factor of 100 greater than for the Junge layer. However, Prinn (1973) has argued that a significant photochemical production rate for  $\text{H}_2\text{SO}_4$  is possible in the atmosphere of Venus. In addition, Samuelson (private communication) and Young (1974) have found that the thermal infrared spectrum of Venus is in good agreement with sulfuric acid cloud particles. We thus conclude, primarily on the basis of the refractive index, that the clouds of Venus are probably composed of a strong sulfuric acid solution.

It is no doubt possible to also obtain the appropriate refractive index in the case of some other substances by judiciously adding certain impurities. Hapke (1972), for example, has suggested the possibility of "dirty" hydrochloric acid. But in any event we have obtained a stiff criterion from the polarization which can be used to test any proposed substance which is chemically specified, since  $n_r(\lambda)$  can always be obtained from experiments and theory. To be consistent with the polarization the substance must also be in the form of spheres which are essentially homogeneous. This latter requirement is particularly evident from the rainbow, which becomes increasingly sharp as the wavelength decreases. Thus, undissolved mixtures such as dust and water are excluded, as are particles with a liquid coating on a nucleus which has a different refractive index.

The clouds examined by means of the polarization of reflected solar radiation are the visible clouds of Venus. This cloud layer (or thick haze) occurs high in the atmosphere by terrestrial standards, at a pressure corresponding to the altitude  $\sim 20$  km on Earth. It is of course possible that there are other cloud layers deeper in the atmosphere with quite a different composition. Theoretical calculations of the polarization for a multi-layered atmosphere will still agree with the observations of Venus if the top layer of particles has an optical thickness  $\tau_c \gtrsim 1$  and particles with the physical properties specified above. This lower limit

on  $\tau_c$  can be converted to a lower limit on the total number  $N_c$  of particles in the "polarization clouds" above unit area. Since the size distribution is narrow we may write  $N_c Q_{\text{ext}} \pi a^2 \approx \tau_c \gtrsim 1$ , where  $Q_{\text{ext}} \approx 2$  (van de Hulst, 1957) and  $a \approx 1 \mu\text{m}$ ; thus,  $N_c \gtrsim 2 \times 10^7 \text{ cm}^{-2}$ . With a density  $\rho \approx 1.7 \text{ gm cm}^{-3}$ , appropriate for an approximate 75%  $\text{H}_2\text{SO}_4$  solution, this corresponds to a cloud particle mass  $\gtrsim 10^{-4} \text{ gm cm}^{-2}$ . We do not yet have a reliable measure of the linear thickness of this cloud or haze region. However, it is worth emphasizing that its optical thickness is substantial; the "polarization clouds" are the visible clouds of Venus, not a tenuous upper haze.

Finally, we would like to point out two types of polarization observations which could considerably refine our knowledge of the composition and structure of the Venus clouds. The extension of accurate polarization observations into the infrared ( $\lambda = 1\text{--}4 \mu\text{m}$ ) and ultraviolet ( $\lambda < 0.34 \mu\text{m}$ ) is needed in order to obtain the refractive index in the spectral regions where significant variations are probable. This would allow a definite identification of the cloud particle composition. In addition, observations in the UV and visible regions with a high spatial resolution could be used to obtain the vertical and horizontal distributions of cloud particles. To obtain the complete potential information would require observations of a given point on the planet from several different zenith angles, as could be obtained from an orbiting spacecraft.

*Acknowledgments.* We would like to thank D. Coffeen, H. Loman, H. C. van de Hulst and A. Young for helpful discussions and R. Jastrow for his hospitality at the Institute for Space Studies.

One of us (J.E.H.) was supported during the course of part of this work by NASA Grant 33-008-012 through Columbia University; the other (J.W.H.) was supported by the Netherlands Organization for the Advancement of Pure Research during a one-year stay at the Institute for Space Studies in 1970-71 when this work was originated.

## APPENDIX

### Anisotropic Rayleigh Scattering

The scattering by molecules was approximated by isotropic Rayleigh scattering in the calculations for the graphs presented in this paper. Although many molecules, particularly  $\text{CO}_2$ , are not isotropic, we show here that anisotropy has only a slight effect on the cloud-top pressure which we deduce from the polarization and also a negligible effect on our other conclusions. Anisotropy reduces the degree of polarization for single scattering, but the effect of this is practically canceled by a comparable increase in the molecular scattering cross section.

#### a. Phase matrix

The phase matrix for anisotropic Rayleigh particles in random orientation is

$$\mathbf{P}_R(\alpha) = \Delta \mathbf{P}_{IR}(\alpha) + (1 - \Delta) \mathbf{P}_I, \quad (\text{A1})$$

where

$$\mathbf{P}_{IR}(\alpha) = \begin{Bmatrix} \frac{3}{4}(1 + \cos^2\alpha) & -\frac{3}{4}\sin^2\alpha & 0 \\ -\frac{3}{4}\sin^2\alpha & \frac{3}{4}(1 + \cos^2\alpha) & 0 \\ 0 & 0 & \frac{3}{2}\cos\alpha \end{Bmatrix} \quad (\text{A2})$$

is the phase matrix for isotropic Rayleigh scattering,

$$\mathbf{P}_I = \begin{Bmatrix} 1 & 0 & 0 \\ 0 & 0 & 0 \\ 0 & 0 & 0 \end{Bmatrix} \quad (\text{A3})$$

is the phase matrix for isotropic scattering,

$$\Delta = \frac{1 - \delta}{1 + \delta/2}, \quad (\text{A4})$$

and  $\delta$ , the so-called depolarization factor, is the ratio of intensities parallel and perpendicular to the plane of scattering ( $I_{\parallel}/I_{\perp}$ ) for light single scattered at  $\alpha = 90^\circ$  with the incident light unpolarized. The above phase matrix is referred to the Stokes parameters  $\{I, Q, U\}$ . A derivation of the phase matrix is given, for example, by Chandrasekhar (1950), though for a different set of Stokes parameters. Measured values of  $\delta$  are given by Penndorf (1957) for a number of gases; some values are  $\text{H}_2 \sim 0.02$ ,  $\text{N}_2 \sim 0.03$ ,  $\text{air} \sim 0.03$ ,  $\text{O}_2 \sim 0.06$  and  $\text{CO}_2 \sim 0.09$ .

From the above equations we find that for anisotropic Rayleigh scattering the degree of linear polarization is

$$\frac{\sin^2\alpha}{1 + \cos^2\alpha + \left(\frac{2\delta}{1 - \delta}\right)} \quad (\text{A5})$$

for single scattering of unpolarized incident light. Thus, it is clear that anisotropy reduces the degree of polarization at all scattering angles, while the general shape as a function of scattering angle remains about the same.

#### b. Scattering coefficient

The scattering coefficient per unit length for anisotropic molecules in random orientation is

$$k_{\text{sca}} = \frac{8\pi^3 (n_g^2 - 1)^2}{3 \lambda^4 N} \frac{6 + 3\delta}{6 - 7\delta}, \quad (\text{A6})$$

where  $N$  is the number of molecules per unit volume,  $n_g$  the refractive index of the gas, and the last factor arises from the anisotropy. A derivation of (A6) is also given by Chandrasekhar (1950). For a mixture of gases

$$k_{\text{sca}} = \frac{8\pi^3}{3\lambda^4 N} \sum_i v_i (n_{g,i}^2 - 1)^2 \frac{6 + 3\delta_i}{6 - 7\delta_i}, \quad (\text{A7})$$

where  $n_{\theta,i}$ ,  $\delta_i$  and  $v_i$  are respectively the refractive index, depolarization factor, and fraction by volume of gas  $i$ .

### c. $p$ - $\tau$ relation

A relation between atmospheric pressure and the optical thickness due to Rayleigh scattering can be derived as follows. Outside of absorption bands the Rayleigh optical thickness due to the gaseous atmosphere above height  $h$  is

$$\tau_R(h) = \int_h^\infty \kappa_{\text{scat}} \rho dh', \quad (\text{A8})$$

where  $\rho$  is the density of gas and  $\kappa_{\text{scat}}$  the scattering coefficient of the molecules per unit mass. Assuming hydrostatic equilibrium, the pressure at height  $h$  is

$$p(h) = \int_h^\infty g \rho dh', \quad (\text{A9})$$

where  $g$  is the acceleration of gravity. Throughout the bulk of the atmosphere the dependence of  $\kappa_{\text{scat}}$  and  $g$  on height can be neglected; thus,

$$p = \frac{g \tau_R}{\kappa_{\text{scat}}}. \quad (\text{A10})$$

Since  $\kappa_{\text{scat}} = \kappa_{\text{scat}} \rho$  and  $\rho = \bar{\mu} N$ , where  $\bar{\mu}$  is the mean molecular mass,

$$p = g \bar{\mu} \tau_R \left[ \frac{8\pi^3}{3\lambda^4 N^2} \sum_i v_i (n_{\theta,i}^2 - 1)^2 \frac{6 + 3\delta_i}{6 - 7\delta_i} \right]^{-1}. \quad (\text{A11})$$

Values for the temperature and pressure dependent quantities in the brackets can be taken for any set of conditions (e.g., for STP, in which case  $N$  is equal to Loschmidt's number).

### d. Application to Venus

If we neglect molecular anisotropy (i.e., if we take  $\delta=0$ ) and assume a pure  $\text{CO}_2$  atmosphere, (A11) leads to

$$p(\text{in bars}) \approx 1.16 \tau_R(0.365 \mu\text{m}), \quad (\text{A12})$$

where  $\tau_R(0.365 \mu\text{m})$  is the Rayleigh optical thickness at  $\lambda = 0.365 \mu\text{m}$ . In obtaining (A12) we took  $N = 2.687 \times 10^{19} \text{ cm}^{-3}$ ,  $g = 870 \text{ cm sec}^{-2}$ ,  $\bar{\mu} = 44 \times 1.66 \times 10^{-24} \text{ gm}$  and  $n_{\theta} \approx 1.00046$  (cf. Allen, 1963, p. 87).

Eq. (A12) corresponds to (14) which gives the pressure  $p_1$  at the level where the cloud optical depth is unity. Since the total polarization arises primarily from the region where the total  $\tau \lesssim 1$ ,  $p_1$  is also approximately the pressure at the  $\tau = 1$  level even if the atmosphere of Venus does not approximate a homogeneous mixture of particles and gas. Thus,  $p_1$  can be termed the cloud-top pressure.

Now consider the case of anisotropic Rayleigh scattering. For a given number of molecules, and thus for a given pressure, anisotropy increases the molecular optical thickness by the factor

$$\frac{1}{1 + \frac{\delta}{2}} \cdot \frac{7}{1 - \frac{\delta}{6}}. \quad (\text{A13})$$

This corresponds to  $\sim 1.17$  for the case of pure  $\text{CO}_2$ , assuming  $\delta(\text{CO}_2) = 0.09$ . However, (A5) shows that anisotropy also decreases the degree of polarization for single scattering by the factor

$$\frac{1 + \cos^2 \alpha}{1 + \cos^2 \alpha + \frac{2\delta}{1 - \delta}}. \quad (\text{A14})$$

This corresponds to  $\sim 0.83$  for  $\delta = 0.09$  and  $\alpha = 90^\circ$ , and it depends little on  $\alpha$ . The product of the above two factors is within a few percent of unity for all relevant phase angles, i.e.,  $\sim 40^\circ$ - $140^\circ$ .

Thus, molecular anisotropy should have little effect on our determination of the atmospheric pressure level at the cloud top. We have verified this by making sample computations with the complete anisotropic Rayleigh phase matrix (A1). The results obtained with anisotropic Rayleigh scattering with  $\delta = 0.09$  do not differ from those for isotropic Rayleigh scattering with the same number of molecules by more than the thickness of the lines in Figs. 9 and 11.

### REFERENCES

- Allen, C. W., 1963: *Astrophysical Quantities*. London, Athlone Press, 291 pp.
- Arking, A., and J. Potter, 1968: The phase curve of Venus and the nature of its clouds. *J. Atmos. Sci.*, **25**, 617-628.
- Avduevsky, V. S., M. Ya. Marov, B. E. Moshkin and A. P. Ekonomov, 1973: Venera 8: Measurements of solar illumination through the atmosphere of Venus. *J. Atmos. Sci.*, **30**, 1215-1218.
- Batsanov, S. S., 1961: *Refractometry and Chemical Structure*. New York, Consultants Bureau, 250 pp.
- Born, M., and E. Wolf, 1965: *Principles of Optics*. London, Pergamon Press, 808 pp.
- Boyer, C., and H. Camichel, 1961: Observations photographiques de la planète Vénus. *Ann. Astrophys.*, **24**, 531-535.
- , and P. Guerin, 1969: Etude de la rotation rétrograde, en 4 jours, de la couche extérieure nuageuse de Vénus. *Icarus*, **11**, 338-355.
- Bryant, H. C., and A. J. Cox, 1966: Mie theory and the glory. *J. Opt. Soc. Amer.*, **56**, 1529-1532.
- Chamberlain, J. W., and G. R. Smith, 1970: Interpretation of the Venus  $\text{CO}_2$  absorption bands. *Astrophys. J.*, **160**, 755-765.
- Chandrasekhar, S., 1950: *Radiative Transfer*. London, Oxford University Press, 393 pp.
- Coffeen, D. L., 1968: A polarimetric study of the atmosphere of Venus. Ph.D. thesis, University of Arizona, 116 pp.

- , 1969: Wavelength dependence of polarization. XVI. Atmosphere of Venus. *Astron. J.*, **74**, 446–460.
- , and T. Gehrels, 1969: Wavelength dependence of polarization. XV. Observations of Venus. *Astron. J.*, **74**, 433–445.
- , and J. E. Hansen, 1973: Polarization studies of planetary atmospheres. *Planets, Stars, and Nebulae Studied with Photopolarimetry*. Tucson, University of Arizona Press, 1133 pp.
- , and L. P. Whitehill, 1974: Polarization of sunlight reflected by terrestrial clouds: Observations and interpretation. To be submitted to *J. Atmos. Sci.*
- Collins, D. G., W. G. Blättner, M. B. Wells and H. G. Horak, 1972: Backward Monte Carlo calculations of the polarization characteristics of the radiation emerging from spherical-shell atmospheres. *Appl. Opt.*, **11**, 2684–2696.
- Cruikshank, D. P., and A. B. Thomson, 1971: On the occurrence of ferrous chloride in the clouds of Venus. *Icarus*, **15**, 497–503.
- Dauvillier, A., 1956: Sur la nature des nuages de Vénus. *Comp. Rend.*, **243**, 1257–1258.
- Deirmendjian, D., 1964: Scattering and polarization properties of water clouds and hazes in the visible and infrared. *Appl. Opt.*, **3**, 187–196.
- Diels, O., and P. Blumberg, 1908: Über das Kohlensuboxyd. *Chem. Ber.*, **41**, 82–86.
- Dollfus, A., 1966: Contribution au Colloque Caltech-JPL sur la lune et les planètes: Venus. Jet Propulsion Laboratory Tech. Memo. No. 33–266, 187–202.
- , 1968: Synthesis on the ultraviolet survey of clouds in Venus' atmosphere. *The Atmospheres of Venus and Mars*, J. C. Brandt and M. E. McElroy, Eds., New York, Gordon and Breach, 133–146.
- , and D. L. Coffeen, 1970: Polarization of Venus. I. Disk observations. *Astron. Astrophys.*, **8**, 251–266.
- Donahoe, F. J., 1970: Is Venus a polywater planet? *Icarus*, **12**, 424–430.
- Elterman, L., R. B. Toolin and J. D. Essex, 1973: Stratospheric aerosol measurements with implications for global climate. *Appl. Opt.*, **12**, 330–337.
- Fahlen, T. S., and H. C. Bryant, 1968: Optical back scattering from single water droplets. *J. Opt. Soc. Amer.*, **58**, 304–310.
- Fjeldbo, G., A. J. Kliore and V. R. Eshleman, 1971: The neutral atmosphere of Venus as studied with the Mariner V radio occultation experiments. *Astron. J.*, **76**, 123–140.
- Forbes, F. F., 1971: Infrared polarization of Venus. *Astrophys. J.*, **165**, L21–L25.
- Friend, J. P., 1966: Properties of the stratospheric aerosol. *Tellus*, **18**, 465–473.
- Garret, A. B., and S. A. Woodruff, 1951: A study of several physical properties of electrolytes over the temperature range of 25°C to –73°C. *J. Phys. Colloid Chem.*, **55**, 477–490.
- Hanel, R., M. Forman, G. Stambach and T. Meilleur, 1968: Preliminary results of Venus observations between 8 and 13 microns. *J. Atmos. Sci.*, **25**, 586–593.
- Hansen, J. E., 1969: Absorption-line formation in a scattering planetary atmosphere: A test of van de Hulst's similarity relations. *Astrophys. J.*, **158**, 337–349.
- , 1971a: Multiple scattering of polarized light in planetary atmospheres. Part I. The doubling method. *J. Atmos. Sci.*, **28**, 120–125.
- , 1971b: Multiple scattering of polarized light in planetary atmospheres. Part II. Sunlight reflected by terrestrial water clouds. *J. Atmos. Sci.*, **28**, 1400–1426.
- , and A. Arking, 1971: Clouds of Venus: Evidence for their nature. *Science*, **171**, 669–672.
- , and J. W. Hovenier, 1971: The doubling method applied to multiple scattering of polarized light. *J. Quant. Spectros. Radiat. Transfer*, **11**, 809–812.
- , and L. D. Travis, 1974: Light scattering in planetary atmospheres. Submitted to *Space Sci. Rev.*
- Hapke, B., 1972: Venus clouds: A dirty hydrochloric acid model. *Science*, **175**, 748–751.
- Hartecck, P., R. R. Reeves and B. A. Thompson, 1963: Photochemical problems of the Venus atmosphere. NASA TN D-1984, 39 pp.
- Hellwege, A. M., 1962: Flüssigkeiten. *Landolt-Börnstein Zahlenwerte und Funktionen*, Band II, Teil 8. Berlin, Springer-Verlag, 901 pp.
- Horak, H. G., 1950: Diffuse reflection by planetary atmospheres. *Astrophys. J.*, **112**, 445–463.
- , and S. J. Little, 1965: Calculations of planetary reflection. *Astrophys. J. Suppl.*, **11**, 373–428.
- Hovenier, J. W., 1969: Symmetry relationships for scattering of polarized light in a slab of randomly oriented particles. *J. Atmos. Sci.*, **26**, 488–499.
- , 1971: Multiple scattering of polarized light in planetary atmospheres. *Astron. Astrophys.*, **13**, 7–29.
- Hoyle, F., 1955: *Frontiers of Astronomy*. New York, Harper, 360 pp.
- Huffman, P., 1970: Polarization of light scattered by ice crystals. *J. Atmos. Sci.*, **27**, 1207–1208.
- Hunten, D. M., 1968: The structure of the lower atmosphere of Venus. *J. Geophys. Res.*, **73**, 1093–1095.
- , 1971: Composition and structure of planetary atmospheres. *Space Sci. Rev.*, **12**, 539–599.
- , and R. M. Goody, 1969: Venus: The next phase of planetary exploration. *Science*, **165**, 1317–1323.
- Irvine, W. M., 1968: Monochromatic phase curves and albedos for Venus. *J. Atmos. Sci.*, **25**, 610–616.
- , and J. B. Pollack, 1968: Infrared optical properties of water and ice spheres. *Icarus*, **8**, 324–360.
- Jaffé, G., 1928: Dispersion und Absorption. *Handbuch der Experimentalphysik*, XIX, W. Wien and F. Harms, Eds., Leipzig, Akad. Verlag. M.B.H., 430 pp.
- Kaplan, L. D., 1963: Spectroscopic investigation of Venus. *J. Quant. Spectrosc. Radiat. Transfer*, **3**, 537–539.
- Kattawar, G. W., and C. N. Adams, 1971: Flux and polarization reflected from a Rayleigh-scattering planetary atmosphere. *Astrophys. J.*, **167**, 183–192.
- , G. N. Plass and C. N. Adams, 1971: Flux and polarization calculations of the radiation reflected from the clouds of Venus. *Astrophys. J.*, **170**, 371–386.
- Kendall, M. G., and A. Stuart, 1963: *The Advanced Theory of Statistics. I. Distribution Theory*. New York, Hafner, 433 pp.
- Kerker, M., 1969: *The Scattering of Light and Other Electromagnetic Radiation*. New York, Academic Press, 666 pp.
- Khrgian, A., Kh., 1961: *Cloud Physics*. Israel Program Scientific Translation, Jerusalem, 392 pp.
- Knuckles, C. F., M. K. Sinton and W. M. Sinton, 1961: UVB photometry of Venus. *Lowell Obs. Bull.*, **5**, 153–156.
- Kratohvil, J. P., 1964: Light scattering. *Anal. Chem.*, **36**, 458R–472R.
- Kuiper, G. P., 1957: The atmosphere and cloud layer of Venus. *Threshold of Space*. M. Zelickoff, Ed. New York, Pergamon, 342 pp.
- , 1969: Identification of the Venus cloud layers. *Comm. Lunar Planet. Lab.*, No. 101, 1–21.
- Lacis, A. A., and J. E. Hansen, 1974. Atmosphere of Venus: Implications of Venera 8 sunlight measurements. Submitted to *Science*.
- Lazrus, A. L., B. Gandrud and R. D. Cadle, 1971: Chemical composition of air filtration samples of the stratospheric sulfate layer. *J. Geophys. Res.*, **76**, 8083–8088.
- Lewis, J. S., 1968: Composition and structure of the clouds of Venus. *Astrophys. J.*, **152**, L79–L83.
- , 1969: Geochemistry of the volatile elements on Venus. *Icarus*, **11**, 367–385.
- , 1971: Refractive index of aqueous HCl solutions and the composition of the Venus clouds. *Nature*, **230**, 295–296.

- , 1972: Composition of the Venus cloud tops in light of recent spectroscopic data. *Astrophys. J.*, **171**, L75-L79.
- Liou, K. N., 1972: Light scattering by ice clouds in the visible and infrared: A theoretical study. *J. Atmos. Sci.*, **29**, 524-536.
- , and J. E. Hansen, 1971: Intensity and polarization for single scattering by polydisperse spheres: A comparison of ray optics and Mie theory. *J. Atmos. Sci.*, **28**, 995-1004.
- Loskutov, V. M., 1971: Interpretation of polarimetric observations of the planets. *Sov. Astron.—AJ*, **15**, 129-133.
- Lyot, B., 1929: Recherches sur la polarisation de la lumière des planètes et de quelques substances terrestres. *Ann. Observ. Paris (Meudon)*, **8**, 161 pp. [available in English as NASA TT F-187, 1964].
- Marin, M., 1965: Mesures photoélectriques de polarisation à l'aide d'un télescope coudé de 1 m. *Rev. Optique*, **44**, 115-144.
- Mie, G., 1908: Beiträge zur Optik Trüber Medien, speziell kolloidaler Metallösungen. *Ann. Phys.*, **25**, 377-445.
- Minnaert, M., 1954: *Light and Colour*. New York, Dover, 362 pp.
- Mossop, S. C., 1965: Stratospheric particles at 20 km altitude. *Geochim. Cosmochim. Acta*, **29**, 201-207.
- O'Leary, B. T., 1966: The presence of ice in the Venus atmosphere as inferred from a halo effect. *Astrophys. J.*, **146**, 754-766.
- Öpik, E. J., 1961: The aelosphere and atmosphere of Venus. *J. Geophys. Res.*, **66**, 2807-2819.
- , 1962: Atmosphere and surface properties of Mars and Venus. *Progress in the Astronautical Sciences*, S. F. Singer, Ed., Amsterdam, North-Holland, 416 pp.
- Penndorf, R., 1957: Tables of the refractive index for standard air and the Rayleigh scattering coefficient for the spectral region between 0.2 and 20.0  $\mu$  and their application to atmospheric optics. *J. Opt. Soc. Amer.*, **47**, 176-182.
- Prinn, R. G., 1973: A photochemical haze model for the clouds of Venus. *Bull. Amer. Astron. Soc.*, **5**, 300.
- Rasool, S. I., 1970: The structure of Venus clouds—Summary. *Radio Sci.*, **5**, 367-368.
- Rea, D. G., and B. T. O'Leary, 1968: On the composition of the Venus clouds. *J. Geophys. Res.*, **73**, 665-675.
- Robbins, R. C., 1964: The reaction products of solar hydrogen and components of the high atmosphere of Venus—A possible source of the Venusian clouds. *Planet. Space Sci.*, **12**, 1143-1146.
- Rosen, J. M., 1971: The boiling point of stratospheric aerosols. *J. Appl. Meteor.*, **10**, 1044-1046.
- Sagan, C., and J. B. Pollack, 1967: Anisotropic nonconservative scattering and the clouds of Venus. *J. Geophys. Res.*, **72**, 469-477.
- Scott, A. H., and E. J. Reese, 1972: Venus: Atmospheric rotation. *Icarus*, **17**, 589-601.
- Sill, G. T. 1972: Sulfuric acid in the Venus clouds. *Comm. Lunar Planet. Lab.*, No. 171, 191-198.
- Sinton, W. M., 1953: Distribution of temperatures and spectra of Venus and other planets. Ph.D. thesis, The Johns Hopkins University, 123 pp.
- Sobolev, V. V., 1968: An investigation of the atmosphere of Venus. II. *Sov. Astron.—AJ*, **12**, 135-140.
- Timmermans, J., 1960: *The Physico-Chemical Constants of Binary Systems in Concentrated Solutions*, Vol. 4. New York, Interscience, 1332 pp.
- Toon, O. B., and J. B. Pollack, 1973: Physical properties of the stratospheric aerosols. *J. Geophys. Res.*, **78**, 7051-7056.
- van Blerkom, D. J., 1971: Diffuse reflection from clouds with horizontal inhomogeneities. *Astrophys. J.*, **166**, 235-242.
- van de Hulst, H. C., 1957: *Light Scattering by Small Particles*. New York, Wiley, 470 pp.
- , 1963: A new look at multiple scattering. Tech. Rept., Goddard Institute for Space Studies, NASA, New York, 81 pp.
- , and K. Grossman, 1968: *The Atmospheres of Venus and Mars*, J. C. Brandt and M. B. McElroy, Eds., New York, Gordon and Breach, 288 pp.
- Velikovsky, I., 1950: *Worlds in Collision*. New York, Macmillan, 401 pp.
- Veverka, J., 1971: A polarimetric search for a Venus halo during the 1969 inferior conjunction. *Icarus*, **14**, 282-283.
- Wildt, R., 1940: On the possible existence of formaldehyde in the atmosphere of Venus. *Astrophys. J.*, **92**, 247-255.
- Young, A. T., 1973: Are the clouds of Venus sulfuric acid? *Icarus*, **18**, 564-582.
- , 1974: Venus clouds: Structure and composition. Submitted to *Science*.
- Young, L. D. Gray, 1972: High-resolution spectra of Venus—A review. *Icarus*, **17**, 632-658.
- , and A. T. Young, 1973: Comment on "The composition of the Venus cloud tops in light of recent spectroscopic data." *Astrophys. J.*, **179**, L39-L43.